# Large reductions in United States heat extremes found in overshoot simulations with SPEAR

**Zachary M. Labe**[1,2,*], **Thomas L. Delworth**[1], **Nathaniel C. Johnson**[1], **Bor-Ting Jong**[2], **Colleen E. McHugh**[1], **William F. Cooke**[1], **and Liwei Jia**[1]

[1] NOAA/OAR/Geophysical Fluid Dynamics Laboratory, Princeton, NJ, USA

[2] Atmospheric and Oceanic Sciences Program, Princeton University, Princeton, NJ, USA

*E-mail: `zacklabe.climate@gmail.com`

March 2025

**Abstract.** Increases in the intensity and frequency of heatwaves are already evident in the observational record, and these increases are expected to be further amplified in future climate projections with greater radiative forcing. However, it is unclear how temperature extremes will respond regionally to emissions reductions and declines of greenhouse gases later in the 21st century, such as through the implementation of global climate mitigation efforts. Here, we evaluate a set of large ensemble experiments that simulate hypothetical 21st century overshoot scenarios using the GFDL SPEAR climate model. While the two overshoot scenarios include a similar evolution of greenhouse gas reductions, they differ in the timing of this drawdown by about a decade. For this study, we then assess whether differences in the timing of starting climate mitigation influences summertime heat extremes across the contiguous United States (CONUS). By quantifying changes in extreme heat relative to the global mean surface temperature before and after the peak in greenhouse gas concentrations, we find significant decreases in the number of CONUS heat extreme days in response to mitigation. This is further amplified for the earlier overshoot scenario, which suggests a greater benefit (i.e., the time below an extreme temperature threshold) in reducing heat impacts by starting climate change mitigation even in as little as a decade sooner. The reductions in heat extremes are consistent with greater mean precipitation and humidity across most of CONUS for equivalent global warming levels. Changes to the global mean land-sea contrast are also found arising from differences in the rate of surface cooling following the greenhouse gas drawdowns. Our results also emphasize the importance of conducting more coordinated large ensemble modeling experiments to understand the range of possible effects of global climate mitigation efforts on changes to regional extreme events.

*Keywords*: heat extremes, climate mitigation, climate change, climate variability, climate models, regional climate, large ensembles, extremes

Submitted to: *Environ. Res. Climate*

## 1. Introduction

Observational data from around the world shows a broad increase in the number of extreme warm days and a reduced frequency of extreme cold days during the last several decades (Perkins-Kirkpatrick and Lewis, 2020). These temperature trends are found for more than 80% of the regions outlined by the Intergovernmental Panel on Climate Change (IPCC, 2023b; IPCC, 2023d), and subsequently, the increase in the number of unusually warm days is accompanied by more severe heat impacts to human health, infrastructure, and to the environment (Boeck et al., 2010; Garcia-Herrera et al., 2010; Raymond et al., 2020; García-León et al., 2021; Henderson et al., 2022). These risks are further amplified with higher levels of projected global warming, including for some of the most densely populated and vulnerable urban areas (Amengual et al., 2014; Ebi et al., 2018; King and Harrington, 2018; Brown, 2020; Dong et al., 2021; Marcotullio et al., 2021; Domeisen et al., 2023; Thompson et al., 2023; Amnuaylojaroen et al., 2024). Understanding changes in heatwave characteristics is therefore crucial in community-level adaptation and mitigation planning and for aiming to reduce societal impacts to extreme events as a whole. This includes accounting for changes in weather and climate extremes under a wide range of possible realizations of the future, such as those with eventual decreases in radiative forcing (Nature, 2023; Dunne et al., 2024; Meinshausen et al., 2024). Moreover, the influences of internal variability can also act to dampen or accelerate regional trends in heat extremes, and therefore long records are needed to properly sample and attribute the magnitude and variability of these events (Perkins-Kirkpatrick et al., 2017; Suarez-Gutierrez et al., 2018; Deser et al., 2020; Yu et al., 2020; Blanusa et al., 2023; Fischer et al., 2023; Risbey et al., 2023).

The contiguous United States (CONUS) is one such location that has observed a large regional divergence in the rate of warming of summertime temperatures and overall heatwave trends (Portmann et al., 2009; Smith et al., 2013; Grose et al., 2017; Mascioli et al., 2017; NCA4, 2018; Marvel et al., 2023; Labe, Johnson and Delworth, 2024). The physical drivers and characteristics of heat extremes across this area are also quite diverse and vary substantially across geography and different climate zones (Lyon and Barnston, 2017; Yang et al., 2019; Thomas et al., 2020). Although the highest number of severe heatwaves, especially for the Great Plains, occurred during the Dust Bowl era of the 1930s (Peterson et al., 2013; Abatzoglou and Barbero, 2014; Donat et al., 2016), some new metrics of heat hazards do indicate a growing threat from heatwaves on average in more recent years (e.g., Shiva et al., 2019; Keellings and Moradkhani, 2020). For instance, there has been a sharp increase in heatwave events for a number of major cities across the CONUS in the last several decades (Habeeb et al., 2015; Marvel et al., 2023), and in fact, the 5th National Climate Assessment identified that the average heatwave season for 50 large metropolitan areas has grown by about 49 days since the 1960s (Marvel et al., 2023).

Differences in the long-term trends of maximum and minimum daily temperature extremes and their associated heat health impacts vary widely across the United States

(Rennie et al., 2019). Parts of the West have observed the largest relative increase in maximum temperatures during the summer season compared to other parts of the country (Lopez et al., 2018; Zhuang et al., 2021; Wanyama et al., 2023; Labe, Johnson and Delworth, 2024). Nighttime minimum temperatures on the other hand are warming for most areas (Gaffen and Ross, 1999; Lyon and Barnston, 2017; Thomas et al., 2020). The lack of clear long-term daytime warming signal focused over mostly the central CONUS is associated with the so-called "warming hole" (Pan et al., 2004; Kunkel et al., 2006), which is a pattern that has been attributed to a number of potential causes ranging from an acceleration of the hydrologic cycle to land-use feedbacks to anthropogenic aerosol forcing (Meehl et al., 2015; Mueller et al., 2016; Banerjee et al., 2017; Mascioli et al., 2017; Partridge et al., 2018a; Eischeid et al., 2023). Despite this observed warming hole feature, most global climate model (GCM) projections indicate a growing probability for extreme heat across the CONUS under greater radiative forcing (Kunkel et al., 2010; Wobus et al., 2018; Lyon et al., 2019; Eischeid et al., 2023; McHugh et al., 2023), with the number of new record high temperatures far exceeding the potential for new record low temperatures (Meehl et al., 2009; Meehl et al., 2016).

While many previous studies have considered the benefits of lower greenhouse gas emissions on future heat extremes globally (e.g., Ciavarella et al., 2017; Tebaldi and Wehner, 2018) and even for the United States (Chen and Ford, 2021), such as by limiting global warming levels to 1.5°C above pre-industrial (e.g., Schleussner et al., 2016; Dosio et al., 2018; King et al., 2018; Kharin et al., 2018), fewer works have considered the regional effects of sudden drawdowns in greenhouse gas levels (Pfleiderer et al., 2024; Roldán-Gómez et al., 2024). This includes assessment of the potential reversibility of climate hazards in response to overshoot scenarios, where global warming is reversed after temporarily exceeding policy-relevant climate benchmarks. Schleussner et al. (2024) highlighted that reducing the timing and magnitude of peak warming during an overshoot period is critical for limiting regional risks or the unintended triggering of Earth system feedbacks. Given that recent studies have found several potential irreversible impacts (e.g., summer precipitation in the Mediterranean; (Delworth et al., 2022)) and time-lagged indicators like sea level rise (e.g., Kim et al., 2022; Meyer et al., 2022; Santana-Falcón et al., 2023; Schleussner et al., 2024), it is central to use state-of-the-art GCM simulations to better understand the regional climate evolution under different plausible overshoot scenarios (Huntingford and Lowe, 2007; Jones et al., 2024). This includes for high-impact events, like temperature extremes.

For this work, we examine the relative changes in the frequency of heat extreme days across the lower 48 United States during summer in response to variations in projected radiative forcing, as prescribed in a 30-member initial condition ensemble. In particular, we look at these changes in climate scenarios that impose drawdowns in greenhouse gases which are analogous to a future with substantial mitigation efforts. These runs also provide us a more feasible mitigation pathway compared to previous work that addressed climate reversibility in perturbation experiments that mainly increase $CO_2$

and then ramp down (e.g., Wu et al., 2010; Boucher et al., 2012; Wu et al., 2015). We focus on how the timing of the implementation of this hypothetical climate mitigation could influence regional heat extreme days by comparing two overshoot scenarios that only differ in their timing by approximately one decade. To conduct these experiments, we use the NOAA Geophysical Fluid Dynamics Labratory (GFDL) Seamless system for Prediction and EArth system Research Large Ensemble, which has a relatively high spatial resolution (nominally 50 km) and 30 ensemble members in each scenario for diagnosing the internal and external forcing contributions. While we primarily use a metric for quantifying heat extremes based on counting the number of daily maximum temperature days that exceed the 90th percentile from a historical model climatology, we also find similar results across more stringent thresholds for both anomalously warm daytime and nighttime temperatures during the summer season.

In response to the reductions in greenhouse gases, we find a significant decline in the number of heat extreme days across the majority of the United States. This decline is largest across the western United States and smallest over the Southeast. The benefits of earlier climate mitigation are found for many regions through a substantial reduction in the number of summers that exceed the maximum count of heat extreme days when comparing the earlier overshoot simulation from the later one. Lastly, we briefly investigate the potential mechanisms associated with the regional temperature anomalies and find that this could be related to the rate of cooling over land compared to the ocean and hence the overall land-sea thermal contrast.

## 2. Data and Methods

### *2.1. SPEAR Large Ensemble Simulations*

We use a collection of large ensemble simulations conducted with the GFDL SPEAR model (Delworth et al., 2020), which is a fully-coupled climate model that was optimized for seamless use in climate prediction and projection. In addition to the uninitialized climate change projections, real-time seasonal and decadal forecasts are regularly produced using SPEAR (Delworth et al., 2020; Lu et al., 2020; Yang et al., 2021), including those that contribute to the North American Multi-Model Ensemble (Kirtman et al., 2014). Aside from a small change in surface albedo over glacial areas (Milly et al., 2014), the land-atmosphere physics of SPEAR are the same as the GFDL LM4-AM4 model components (Zhao et al., 2018a; Zhao et al., 2018b), which were used as part of GFDL's coupled climate model CM4 (Held et al., 2019). SPEAR also includes the MOM6 ocean and SIS2 sea ice code (Adcroft et al., 2019). The atmosphere contains 33 vertical levels up to a model top of 1 hPa, and the land-atmosphere horizontal resolution of this configuration is approximately 50 km. The ocean contains 75 vertical levels, and its grid features a nominal resolution of 1°, but with a refinement to 0.33° in the deep tropics for improved tropical climate variability.

The large ensemble simulations evaluated here include 30 individual ensemble members for each historical and future scenario (Table S1), which is helpful for characterizing internal climate variability and sampling a wider distribution of possible extreme events in the model (Deser et al., 2020; Jain et al., 2023). Consequently, the range of internal variability in each SPEAR simulation can be assessed through the spread across all ensemble members, and the ensemble mean is then assumed to be attributable to external forcing (Deser et al., 2012; Phillips et al., 2020). The historical ensemble members are launched using initial conditions from restart files that are spaced 20 years apart from an 1850 control run with SPEAR, but all ensemble members share the same land initial conditions. These land conditions are created through a 1-year run after a 300-year spin-up. Boundary conditions and natural and anthropogenic forcings (e.g., aerosols, greenhouse gases, land use/land change, solar irradiance) follow the historical Coupled Model Intercomparison Project Phase 6 (CMIP6; Eyring et al., 2016; Meinshausen et al., 2017; Hurtt et al., 2020) conventions over the years from 1921 to 2014. Afterwards, starting in 2015, SPEAR is prescribed with time-evolving projected radiative forcing from a set of Shared Socioeconomic Pathways (SSPs; O'Neill et al., 2014; O'Neill et al., 2016; O'Neill et al., 2017; Meinshausen et al., 2020) through 2100 (Table S1). For this work, we focus on radiative forcing following the SSP2-4.5, SSP5-8.5, and SSP5-3.4OS future scenarios (Kriegler et al., 2017; Riahi et al., 2017; Gidden et al., 2019; Tebaldi et al., 2021) (Figure 1 and Table S1). An additional simulation is considered following radiative forcing change similar to SSP5-3.4OS, but with carbon dioxide and methane concentrations scaled to begin declining approximately 10 years earlier (SSP5-3.4OS_10ye; see Labe, Delworth, Johnson and Cooke, 2024) (Figure 1a-b). By 2100, this leads to carbon dioxide and methane levels of approximately 68 ppm and 111 ppb less than SSP5-3.4OS, respectively. The relevance of the SSP5-3.4OS_10ye scenario will be discussed more below. Both SSP5-3.4OS and SSP5-3.4OS_10ye scenarios also simulate carbon dioxide and methane concentrations that fall below SSP2-4.5 by the middle of the 21st century (Figure 1a-b). The global mean level of nitrous oxide in SSP5-3.4OS_10ye is prescribed to SSP5-3.4OS and is actually 7 ppb higher than SSP2-4.5 by 2100 (Figure 1c), but its overall contribution to global mean warming remains small relative to carbon dioxide and methane (IPCC, 2023a; Tian, Pan, Thompson, Canadell, Suntharalingam, Regnier, Davidson, Prather, Ciais, Muntean, Pan, Winiwarter, Zaehle, Zhou, Jackson, Bange, Berthet, Bian, Bianchi, Bouwman, Buitenhuis, Dutton, Hu, Ito, Jain, Jeltsch-Thömmes, Joos, Kou-Giesbrecht, Krummel, Lan, Landolfi, Lauerwald, Li, Lu, Maavara, Manizza, Millet, Mühle, Patra, Peters, Qin, Raymond, Resplandy, Rosentreter, Shi, Sun, Tonina, Tubiello, Werf, Vuichard, Wang, Wells, Western, Wilson, Yang, Yao, You and Zhu, 2024) and therefore likely does not impact our overall conclusions.

At this stage, the SSP5-8.5 scenario appears to be an unrealistic forcing for future climate impact assessments (e.g., Peters and Hausfather, 2020; Pielke et al., 2022; Hausfather, 2025). We include the analysis of it here only due to the design of SSP5-3.4OS, which itself is a Tier 2 experiment from CMIP6 that follows SSP5-8.5 until 2040 but then introduces rapid reductions in greenhouse gas emissions that lead to negative net emissions after 2070 (O'Neill et al., 2016) (Figure 1a-c). This drawdown in greenhouse gases is due to declining fossil fuel emissions and through carbon capture and storage technology, such as through the inclusion of bioenergy crops for nearly all new cropland areas after mitigation begins (Melnikova et al., 2022). The likelihood of following this exact scenario is rather low but was constructed to begin exploring the effects of climate mitigation and adaptation practices in a large 21st century overshoot, such as for consideration of climate reversibility and hysteresis effects. SSP5-3.4OS eventually leads to a net radiative forcing of 3.4 W $m^{-2}$ by 2100 (Tebaldi et al., 2021). Thus, by comparing results with SSP5-3.4OS and SSP5-3.4OS_10ye radiative forcing, we can assess the impacts of delaying aggressive climate mitigation efforts on extreme events and the large-scale circulation in this idealized setting with SPEAR (Labe, Delworth, Johnson and Cooke, 2024).

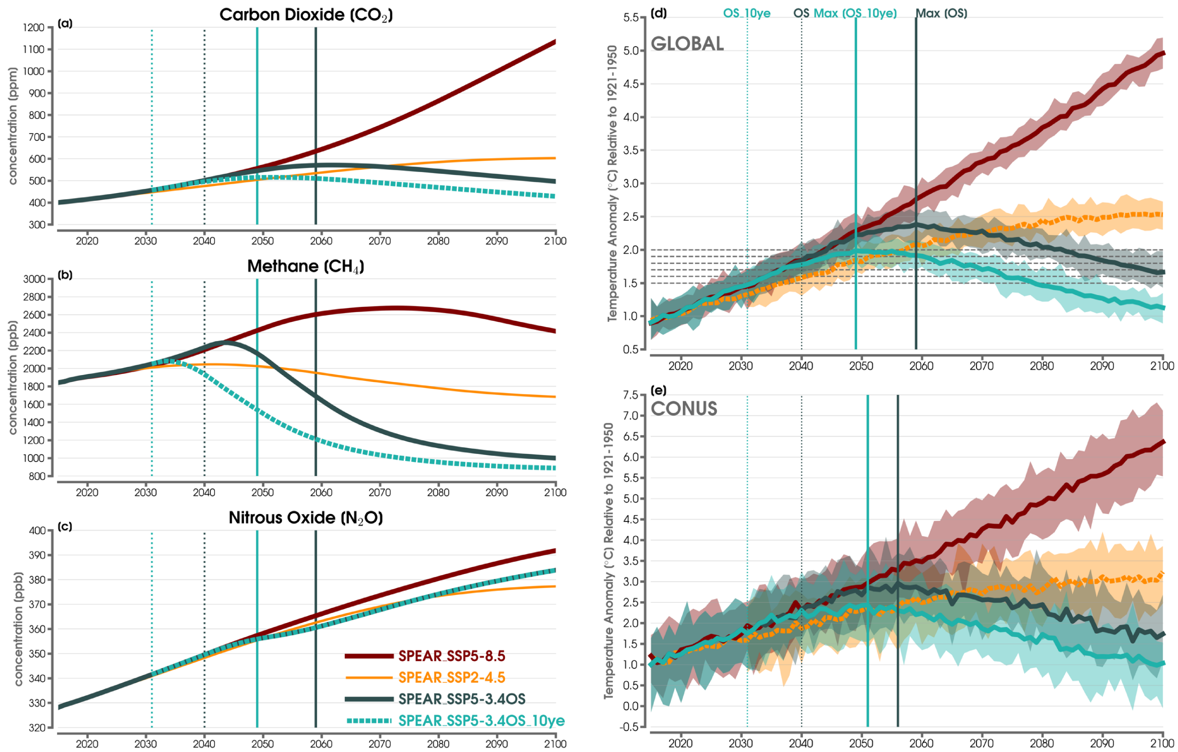


Figure 1: (a) Time series of annual mean carbon dioxide ($CO_2$; parts per million (ppm)) from 2015 to 2100 for the SSP5-8.5 climate scenario of SPEAR (solid red line), SSP2-4.5 (thin orange line), SSP5-3.4OS (solid dark green line), and SSP5-3.4OS_10ye from 2031 to 2100 (dashed light green line). The dashed vertical lines indicate the start of climate mitigation in 2031 (light green) and 2041 (dark green) for SSP5-3.4OS_10ye and SSP5-3.4OS, respectively. The solid vertical lines indicate the maximum ensemble-mean global temperature for SSP5-3.4OS_10ye (light green) and SSP5-3.4OS (dark green), respectively. (b) As in (a), but for methane ($CH_4$; parts per billion (ppb)). (c) As in (a), but for nitrous oxide ($N_2O$; parts per billion (ppb)). (d) Time series of annual mean GMST from 2015 to 2100 for the ensemble mean of SPEAR following SSP5-8.5 (solid red line), SSP2-4.5 (dashed orange line), SSP5-3.4OS (solid dark green line), and from 2031 to 2100 for SSP5-3.4OS_10ye (solid light green line). The spread across SPEAR ensemble members is shown with the lighter shading for each respective experiment. Anomalies are computed with respect to their 1921-1950 climatological time means. The dashed vertical lines indicate the start of climate mitigation in 2031 (light green) and 2041 (dark green) for SSP5-3.4OS_10ye and SSP5-3.4OS, respectively. The solid vertical lines indicate the maximum (max) ensemble-mean global temperature for SSP5-3.4OS_10ye (light green) and SSP5-3.4OS (dark green), respectively. The dashed horizontal grey lines annotate GWLs from 1.5 to 2.0°C at an interval of 0.1°C. (e) Same design as (d), but calculated only over temperatures across the CONUS region.

Peak surface warming in the global mean sense corresponds closely with the maximum in carbon dioxide concentrations (Figure 1a) for both SSP5-3.4OS and SSP5-3.4OS_10ye, which is about 2.38°C (2.23°C to 2.63°C ensemble spread) and 1.99°C (1.82°C to 2.24°C ensemble spread) above the 1921-1950 baseline respectively for each ensemble mean. For SSP5-3.4OS, this is approximately the same as the end of the 21st century global mean surface temperature (GMST) anomaly for SSP2-4.5 (+2.53°C) (Figure 1d), but well below SSP5-8.5 (4.96°C). The timing of this difference in maximum GMST between SSP5-3.4OS and SSP5-3.4OS_10ye is also 10 years (2049 vs. 2059), although the regional temperature and precipitation responses are still found to be clearly distinguishable from that of internal variability (Labe, Delworth, Johnson and Cooke, 2024).

Unsurprisingly, compared to GMST, greater annual mean warming is found when averaged across land areas of CONUS in each future radiative forcing scenario (Figure 1e). The maximum annual mean temperature anomaly for this region is 3.23°C for SSP2-4.5 (2.55°C to 4.20°C ensemble spread), 2.96°C for SSP5-3.4OS (2.26°C to 4.08°C ensemble spread), and 2.43°C for SSP5-3.4OS_10ye (1.88°C to 3.54°C ensemble spread). There is only a difference in 5 years for when this maximum is reached in the overshoot scenarios (2051 vs. 2056), but it is possible this is simply due to greater variability when assessing the forced response using the ensemble mean for much smaller spatial scales (i.e., CONUS). Slightly greater than the difference in GMST, there is about a 0.7°C deviation in the mean CONUS temperature anomaly between the ensemble means of SSP5-3.4OS and SSP5-3.4OS_10ye by the year 2100. Cooling also appears likely to continue if one were to further extend these overshoot simulations beyond 2100, whereas for SSP2-4.5 there is more of a stabilization of mean CONUS temperatures (Figure 1e).

A limitation of this analysis is that we only focus on simulations from one GCM. However, we note that SPEAR has been previously evaluated in a number of heat extreme studies, and the large number of ensemble members available for each radiative forcing scenario at a 50 km atmospheric resolution provide us a unique opportunity to consider the effects of internal variability under these sudden mitigation pathways. For example, SPEAR has been shown to skillfully predict both heat and cold extremes at the seasonal timescale (Jia et al., 2022; Jia et al., 2023; Jia et al., 2024), as well as accurately capturing temperature variability over North America from key El Niño-Southern Oscillation (ENSO) and Pacific Decadal Variability (PDV) teleconnections (Maher et al., 2022; Johnson et al., 2022). The model has also been used for the conditional attribution of observed heatwave events (Schreck et al., 2024) and for evaluation of long-term climate change projections of summertime warmth (Labe, Johnson and Delworth, 2024) and record-breaking daily high temperatures (McHugh et al., 2023) across the CONUS. Note that historical heat extreme comparisons and model biases are already documented for SPEAR relative to station observations and atmospheric reanalysis data and can be found in Jia et al. (2022), McHugh et al. (2023), and Labe, Johnson and Delworth (2024). SPEAR overall has a tendency to overestimate the long-term warming trend across CONUS (McHugh et al., 2023), which at least in summer is related to the central United States warming hole pattern (Pan et al., 2004; Eischeid et al., 2023).

### *2.2. Definitions of Heat Extremes*

For the majority of this study, we use a static definition for heat extremes that is based upon the 90th-percentile of the climatological distribution of daily maximum temperatures (Tx90) for a given reference period (Hamilton et al., 2012; Pepler et al., 2015; Jia et al., 2022). This threshold is calculated separately at each grid point over land areas of the CONUS using daily data from the historical scenario of SPEAR. Our focus is on the boreal summer season of June-July-August (JJA), and we simply count the number (or probability) of JJA days that exceed the Tx90 threshold per each year using the SPEAR large ensemble runs.

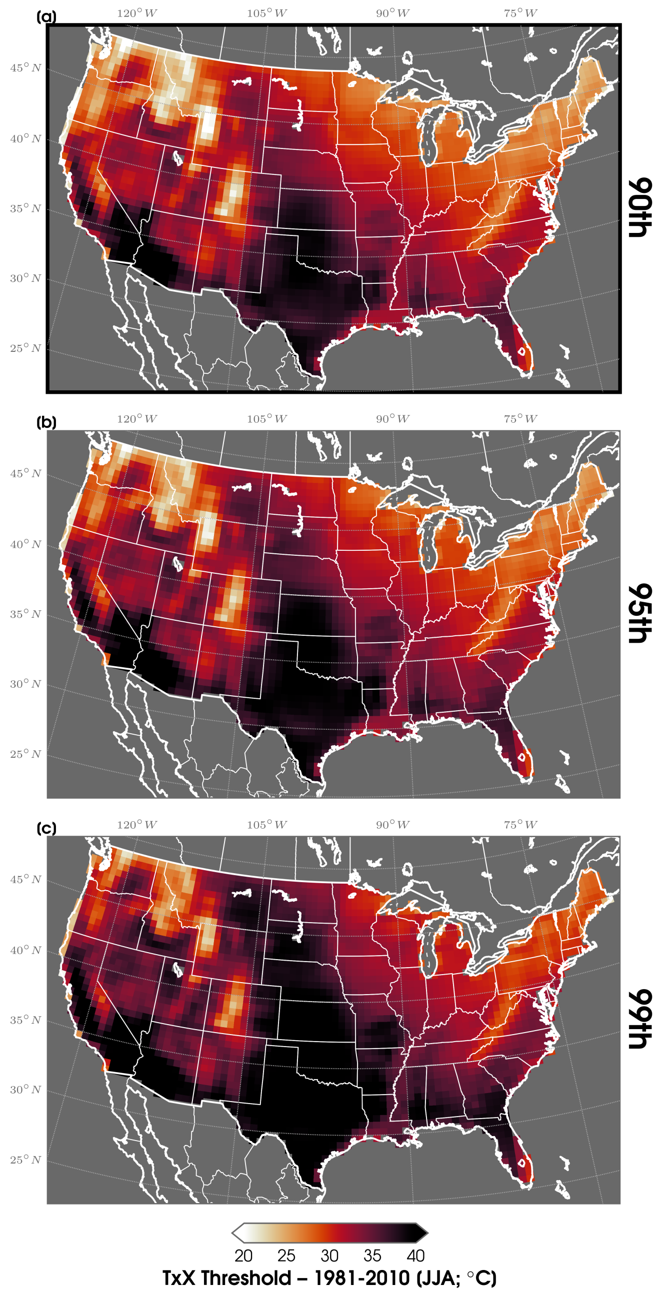


Figure 2: (a) CONUS map of the raw daytime heat extreme thresholds in summer for the 90th percentile (Tx90), 95th percentile (Tx95), and 99th percentile (Tx99). This static threshold is calculated based on the distribution of daily maximum temperatures from June to August and across all 30 ensemble members using the SPEAR historical run from 1981 to 2010. This threshold is computed separately at each grid point.

To calculate each distribution of daily maximum temperatures, all 30 ensemble members and all years from 1981 to 2010 are considered with SPEAR. Following this definition, the Tx90 thresholds are shown in Figure 2a. A comparison of SPEAR with an observed definition of Tx90 can be found in Figure 1 of Jia et al. (2022), but note our focus in this work is predominately to understand the changes in summertime hot days in response to changes in radiative forcing within SPEAR. Given that Tx90 is only a moderately hot heat metric, we also calculate the future exceedance of the 95th- and 99th-percentile of daily maximum temperature days (Figure 2b-c), as well as exceeding the absolute warmest daily maximum temperature in JJA (TXx). Lastly, we also explore changes in the number of warm nighttime temperatures in future JJA seasons, but find quantitatively similar mean results when averaged across the CONUS. We therefore only show these figures in the Supporting Information section, which mirror those shown in the main text for daily maximum heat extremes. For example, the same percentile-based thresholds for the anomalously warm daily minimum temperature days in JJA are calculated and shown in Figure S1. The areas with the warmest daily maximum and minimum temperatures are both found across the southwest and south-central CONUS (Figures 2 and S1)

## 3. Results and Discussion

### *3.1. Projections of Summertime Heat Extremes*

To make an initial assessment of how the frequency of heat extreme days are changing in these different radiative forcing scenarios, we show in Figure 3a the time series of the projected number of days exceeding the 90th percentile in each summer for the CONUS region. Recall that the baseline for calculating these temperature thresholds is 1981-2010. By 2100, the number of Tx90 days ranges from 24 to 48 in SSP2-4.5 and has an ensemble mean of about 38 days. This is also the corresponding maximum count over the entire 2015-2100 period for SSP2-4.5, which is greater than the ensemble mean maximum found for SSP5-3.4OS of 36 days (28-55 day spread) and for SSP5-3.4OS_10ye of 30 days (22-42 day spread). In the overshoot simulations, these maximum ensemble mean counts are respectively reached in 2040 and 2060. The large ensemble spread found in each scenario suggest an important role for internal variability remaining even under the influence of greater external forcing. However, we do find a smaller mean spread for the SSP5-8.5 scenario average of about 15 days from 2015 to 2100 compared to 18-20 days in the three other climate change scenarios. Despite similar projected counts of warm nighttime extremes (Tn90), which are shown in Figure S2, the ensemble spreads are generally smaller than Tx90 and range from an average of 12 (SSP5-8.5) to 16 (SSP2-4.5) days across the four climate scenarios. Figure 3b shows distributions for the CONUS mean number of Tx90 days (and in Figure S2 for Tn90) over 30-year epochs at the end of the 21st century (i.e., 2071-2100) compared to the 1981-2010 historical baseline. Note that the wider PDFs for SSP5-8.5 is due to the sharp increases in Tx90 and Tn90 days evolving through the duration of the simulation. Using the two-sample Kolmogorov-Smirnov test, we find that the Tx90 distributions for the SSP5-3.4OS compared to SSP5-3.4OS_10ye are significantly different ($p < 0.05$) for the 2071-2100 period. The results in Figure 3 thus provide initial evidence for the importance of earlier greenhouse gas mitigation in reducing the number of future Tx90 days. This will be explored in greater detail later on.

As expected, this increase in heat extreme days is due in large part to the rise in the background mean warming over CONUS (e.g. McKinnon et al., 2024), which is displayed in Figure S3b for all four scenarios for the average surface temperature (T2M) during JJA. Warming is notably larger in JJA than for the annual mean (Figure 1e), with, for example, a maximum anomaly, relative to 1981-2010, of 3.95°C under SS2-4.5 (2.77°C to 4.91°C ensemble spread) in year 2100. Similarly, greater ensemble mean JJA warming is simulated for SSP5-3.4OS (3.82°C in 2060) and SSP5-3.4OS_10ye (3.21°C in 2040) before the cooling induced by the drawdown of greenhouse gas concentrations. Comparing this seasonal mean summertime warming to another metric of extremes in Figure S3a, the absolute highest daily maximum temperature during JJA (TXx), we find a fairly similar amount of ensemble mean warming (e.g., 4.04°C for SSP5-3.4OS in 2060) but greater ensemble spread and thus interannual variability. For this CONUS-wide mean metric, a difference in the timing of rapid mitigation leads to an overall ensemble mean difference of 0.82°C in TXx for the 2071-2100 period between SSP5-3.4OS and SSP5-3.4OS_10ye (Figure S3a).

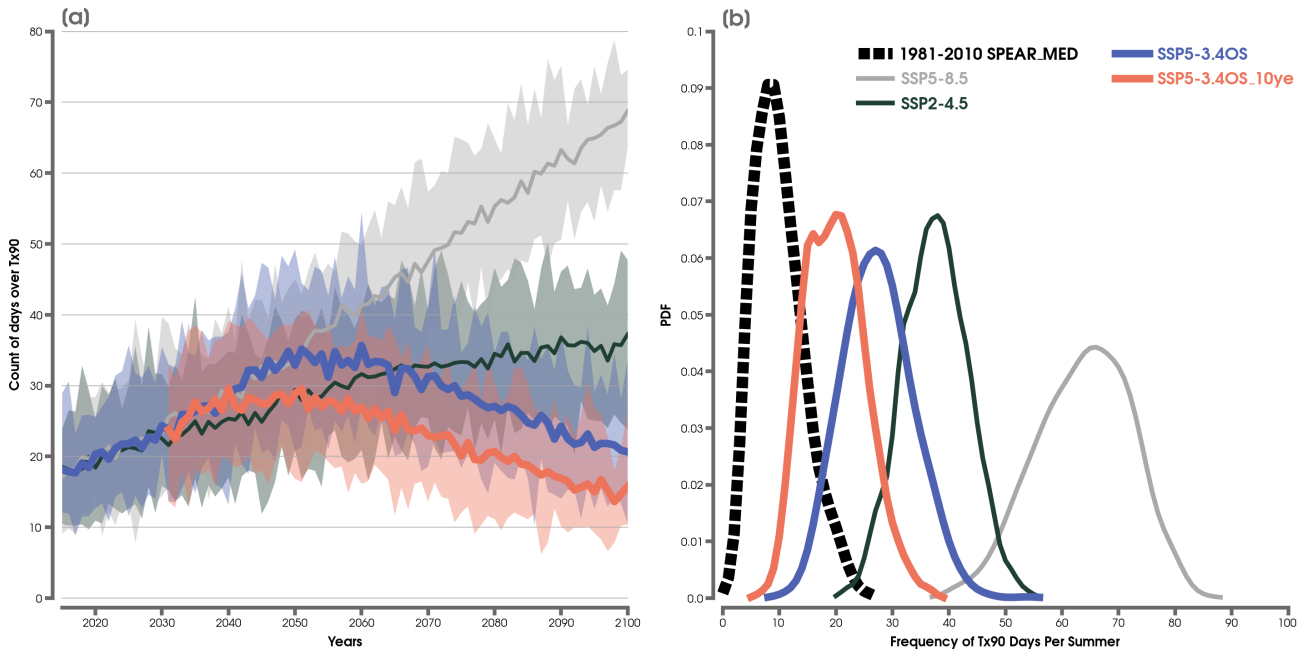


Figure 3: (a) Time series of the count of JJA heat extreme days (Tx90) averaged for CONUS from 2015 to 2100 for the ensemble mean following SSP5-8.5 (light gray line), SSP2-4.5 (dark green line), SSP5-3.4OS (purple line) and from 2031 to 2100 for SSP5-3.4OS_10ye (orange line). The spread across ensemble members is shown with the lighter shading for each respective experiment. (b) Probability density functions (PDFs) of the distribution of the average frequency of mean CONUS Tx90 days in JJA over the years 1981 to 2010 using the historical SPEAR scenario (dashed black curve), SSP5-8.5 from 2071 to 2100 (light gray curve), SSP2-4.5 from 2071 to 2100 (orange curve), SSP5-3.4OS from 2071 to 2100 (dark green curve), and SSP5-3.4OS_10ye from 2071 to 2100 (purple curve). The non-parametric PDFs are constructed using gaussian kernel density estimation with the optimal bandwidth determined through cross-validation. Each PDF considers data from all ensemble members in each 30-year period.

To better understand the spatial patterns of heat extreme day anomalies, we show composites of changes in Tx90 days during JJA at a global warming level (GWL) of 1.7°C for SSP5-8.5, which occurs in 2037, in Figure 4a. Here we calculate this composite based on an epoch of ±2 years around when the 30-member ensemble-mean, annual mean GMST anomaly reaches 1.7°C above the 1921-1950 reference period. Due to the start of the SPEAR historical simulation beginning in 1921 which is later than the standard pre-industrial period, we acknowledge that our GWL reference period differs from the 1850-1900 mean that is traditionally used for climate policy and decision-making (IPCC, 2021). However, recall that our primary interest is for understanding the overall Tx90 response before and after the drawdown in greenhouse gas levels in the relatively idealized overshoot simulations. In other words, we consider the reversibility of such a response in summertime heat extremes. Assessing climate projections as a function of GWL also helps to reduce scenario-dependent uncertainties (see Cross-Chapter Box 11.1 in IPCC, 2023d) and can be useful when accounting for alternative pathways like those following hypothetical mitigation (James et al., 2017). This framing is generally not forcing-dependent for temperature extremes (Seneviratne and Hauser, 2020; Wehner, 2020), and GWLs have been widely used for assessing projected changes in future heatwaves (e.g., Fischer and Knutti, 2015; Schleussner et al., 2016; Perkins-Kirkpatrick and Gibson, 2017; Suarez-Gutierrez et al., 2020), including across the CONUS (e.g., Wobus et al., 2018; Marvel et al., 2023).

Corresponding to a GWL of 1.7°C in SSP5-8.5, increases in the number of days exceeding Tx90 are visible across all of the CONUS (Figure 4a). The largest rises are found across the higher elevations of the West, southeastern Florida, and the central Appalachians with the number of heat extreme days increasing by 20-50 days per summer. A local minimum for changes in Tx90 days is shown over the Southeast, which interestingly closely mirrors portions of the warming hole found in real-world observations (Rogers, 2013; Partridge et al., 2018b; Ghate et al., 2022; Eischeid et al., 2023). The driver of this warming minimum found in the SPEAR ensemble mean remains unclear (McHugh et al., 2023; Labe, Johnson and Delworth, 2024), but there is some preliminary evidence that the anomaly may be related to local land-atmosphere interactions simulated by the model (not shown).

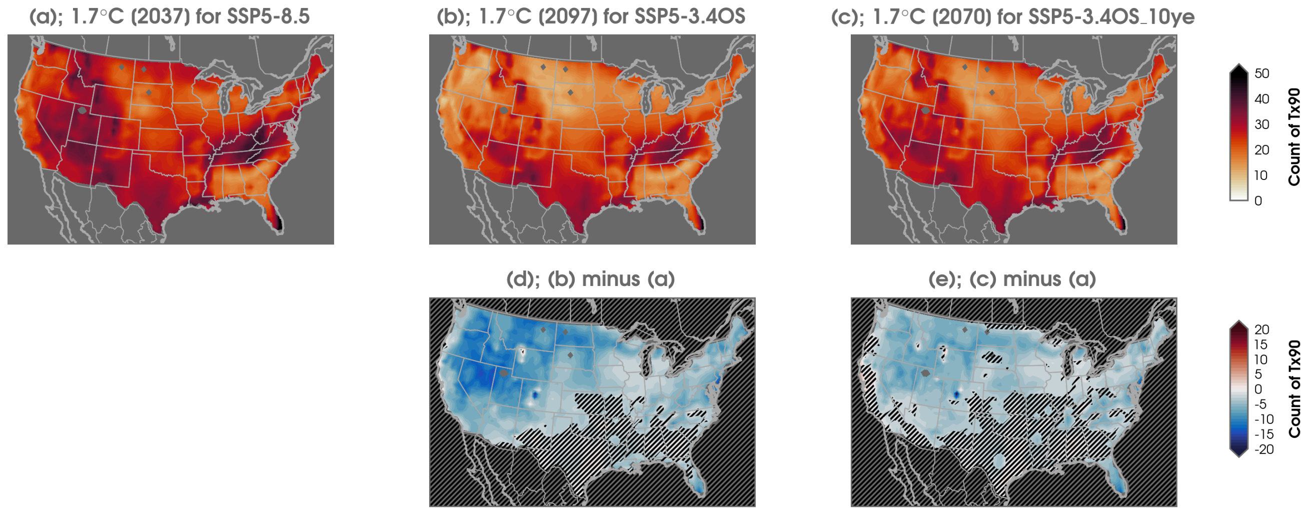


Figure 4: (a) Change in the number of Tx90 days at a GWL of 1.7°C for the SSP5-8.5 climate scenario. (b) Same as (a), but for SSP5-3.4OS after the influences of climate mitigation efforts are underway (see text for details). (c) Same as (b), but for SSP5-3.4OS_10ye. (d) Difference in panel (b) minus (a). (e) Difference in panel (c) minus (a). All anomalies are computed with respect to the 1921-1950 climatological time means from the SPEAR historical scenario. Each composite map is calculated as the average of ±2 years around the ensemble mean year closest to an annual mean GMST change of 1.7°C per climate scenario, with the central year indicated above panels a, b, and c. Statistically significant differences in panels (d) and (e) are shown with the anomaly color shading. Non-significant regions are denoted with black hatching, which is assessed using a two-sided Student's $t$ test and after adjusting for field significance using a false discovery rate (FDR; Benjamini and Hochberg, 1995; Wilks, 2006; Wilks, 2016) (i.e., a FDR-adjusted $p$-value less than 0.05).

Next, to assess the regional response of heat extremes *after* peak greenhouse levels for the two respective overshoot runs, Figure 4b-c shows Tx90 changes at an approximately equivalent level of mean GMST warming. The choice of focusing on the GWL equal to 1.7°C is more obvious here, since the GMST in SSP5-3.4OS falls below this GWL threshold just before the end of the century (i.e., about year 2097; Figure 4b). Thus, an ensemble mean GMST of 1.7°C is observed before and after peak greenhouse gas concentrations in both SSP5-3.4OS and SSP5-3.4OS_10ye. This does not occur again for a GMST anomaly of 1.5°C in SSP5-3.4OS through at least 2100, as demonstrated by the horizontal gray dashed lines that are annotated in Figure 1d. Though we do find quantitatively similar results when reproducing Figure 4 for other composites of different GWLs (such as 1.8°C; not shown).

For these overshoot composites in Figure 4b-c, we find a similar spatial pattern of Tx90 day anomalies, but a notable reduction in the number of days. This decrease is more clearly displayed in Figure 4d-e by taking the difference in the Tx90 anomalies for each overshoot scenarios during the ramp down in greenhouse gases relative to the SSP5-8.5 composite at the same GWL. A statistically significant decrease in the number of Tx90 days, up to two weeks, is found for SSP5-3.4OS and SSP5-3.4OS_10ye across much of the region outside of the south-central United States. The largest reduction is apparent over the Western United States, particularly for SSP5-3.4OS (Figure 4d).

An analogous view for Tn90 days can be found in Figure S4. While all areas observe an increase in anomalously warm minimum temperatures at a GWL of 1.7°C (Figure S4a-c), there is a CONUS-wide net decrease in the magnitude of days exceeding Tn90 in the overshoot scenarios after peak global warming. This difference is most amplified again across the West with up to a week fewer Tn90 days (Figure S4d-e). Also, in contrast to the regional minimum in Tx90 days over the Southeast (Figure 4a-c), we find greater Tn90 days here relative to other parts of CONUS. Overall, these Tx90 and Tn90 composite results suggest that even at the same level of mean global warming, there are substantially faster reductions in the frequency of heat extremes when comparing the scenarios before versus and aggressive climate mitigation. This will be the focus of the remaining analysis.

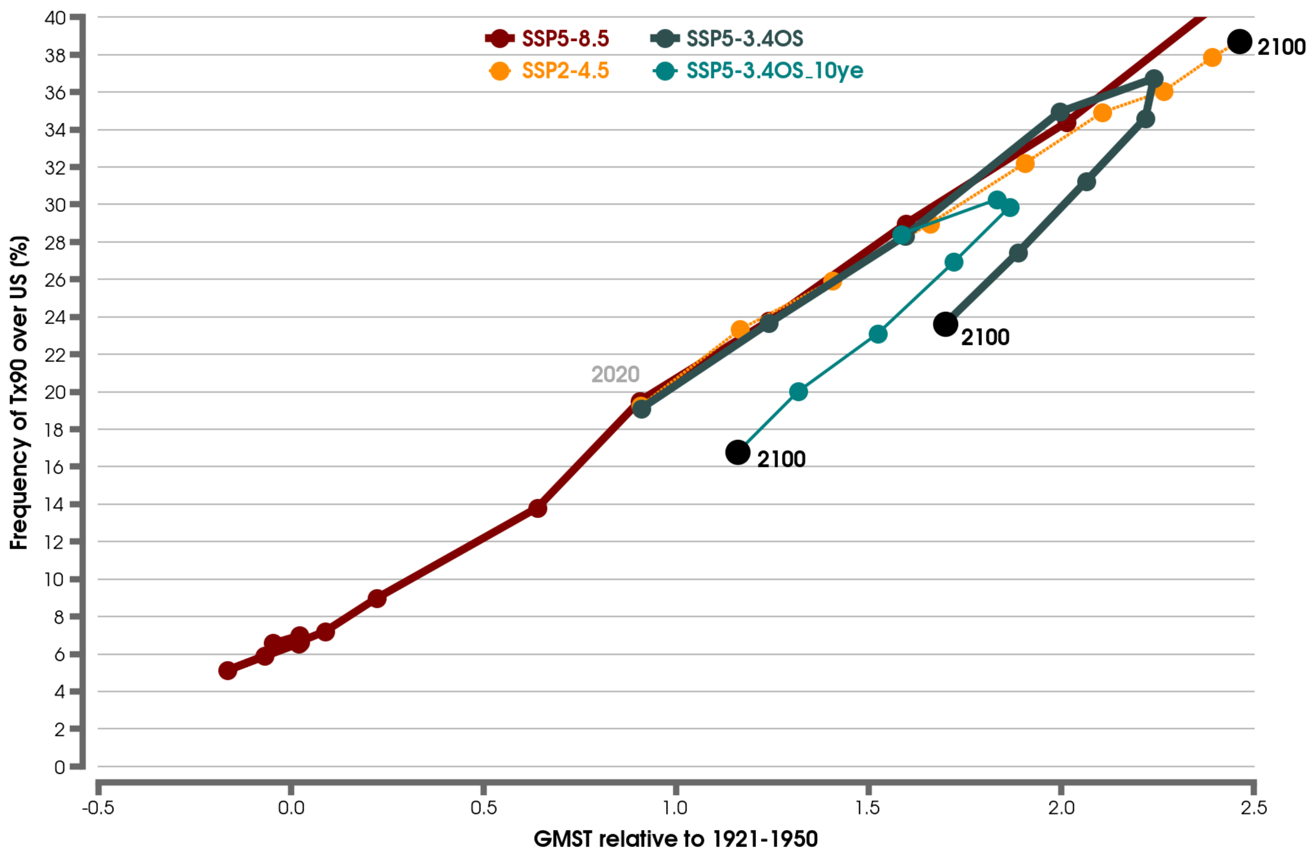


Figure 5: Decadal average frequency of JJA Tx90 heat extreme days averaged across the CONUS as a function of JJA mean GMST for the same future climate scenarios shown in Figure 1. GMST anomalies are computed with respect to the 1921-1950 climatological time mean. The historical climate scenario is used to calculate the decadal means starting in 1921 and then is concatenated with each future scenario beginning in 2015. The black scatter points indicate the final decade of analysis (e.g., where 2100 is calculated as 2091-2100) in each climate scenario. Note that the frequency of SSP5-8.5 heat extremes extend well beyond the graph (see Figure S5).

Figure 5 scales the transient mean CONUS response of Tx90 day frequency by GMST for the decadal averages in the historical, SSP5-8.5, SSP2-4.5, and two overshoot runs. This scaling approach has been used in multiple studies to understand the regional climate sensitivity to changes in extremes (e.g., Seneviratne et al., 2016; Wartenburger et al., 2017; Seneviratne and Hauser, 2020), including for land temperatures in a multi-model collection of CMIP6 overshoot runs (Roldán-Gómez et al., 2024). Similar to these previous studies, we find a mostly linear effect of ensemble mean Tx90 days as a function of mean global warming, although this response accelerates slightly for SSP5-8.5 with more intense hot days (Tx99) and greater overall warming compared to the other emission scenarios (Figure S5). For both average CONUS Tx90 and Tx99, we find a different relationship with GMST after peak warming in the ensemble means of SSP5-3.4OS and SSP5-3.4OS_10ye. This follows by an increasing rate of cooling, which is especially evident for SSP5-3.4OS and corresponds to an approximately 5-8% reduction in Tx90 frequency for equivalent levels of global warming compared to before the peak in emissions (SSP5-8.5 line).

### *3.2. Variability of Future Heat Extreme Risk*

While we have primarily focused on the reversibility of heat extremes in the ensemble mean, Figure 3 also highlights a large range in responses resulting from the effects of internal variability, and thus, this a key source of uncertainty in terms of projecting climate impacts for society. Figure 6 instead shows more probabilistic assessment and identifies the chance of having at least one month with a day that exceeds the absolute highest maximum temperature (TXx) in JJA (1981-2010) within all ensemble members for the SSP5-8.5, SSP5-3.4OS, and SSP5-3.4OS_10ye scenarios. These probabilities are calculated separately by 10 to 15-year periods evolving from 2015 to 2100 and at each individual grid point. Despite the somewhat wide and overlapping ensemble spreads in mean CONUS-wide TXx, as shown in Figure S3a, we again find substantial differences between SSP5-3.4OS and SSP5-3.4OS_10ye (Figure 6g-r). Although the drawdown of carbon dioxide and methane is well underway for both overshoot scenarios by the 2060-2074 epoch, we see many regions with a 5-10% lower probability (up to 19%) of historical TXx exceedance in 2060-2074 for SSP5-3.4OS_10ye compared to SSP5-3.4OS (i.e., comparing Figure 6p to Figure 6j). Then, by the end of the 21st century, this chance drops to nearly 0% across the CONUS in response to the climate mitigation efforts.

As expected with substantially higher radiative forcing, the probability of having a month exceeding the historical TXx largely increases for SSP5-8.5 (Figure 6a-f). By 2075-2089, this probability reaches at least 50% across large sections of the country. Parts of the Southwest and eastern CONUS even see probabilities reaching up to 98% when considering across all months and ensemble members in 2090-2100 (Figure 6f). In contrast, the highest probability for exceeding the historical JJA TXx threshold is set in 2060-2074 for SSP5-3.4OS for exceeding their historical JJA TXx threshold, and this is only about a 28% chance over a small area in the Southwest. In SSP5-3.4OS_10ye, we see the absolute highest TXx probability drop to a maximum of 17%, which is in 2030-2044 for western Colorado (Figure 6n). Once again there is very large spatial variability in the magnitude of these probabilities; for instance, we see notably less intense heat extremes in the Southeast relative to the rest of CONUS, even for SSP5-8.5 (Figure 6c-f). Another local minimum is found across northern California, Oregon, and Washington, but this may be a product of the already accelerated warming simulated by SPEAR during the historical reference period across these regions (Labe, Johnson and Delworth, 2024).

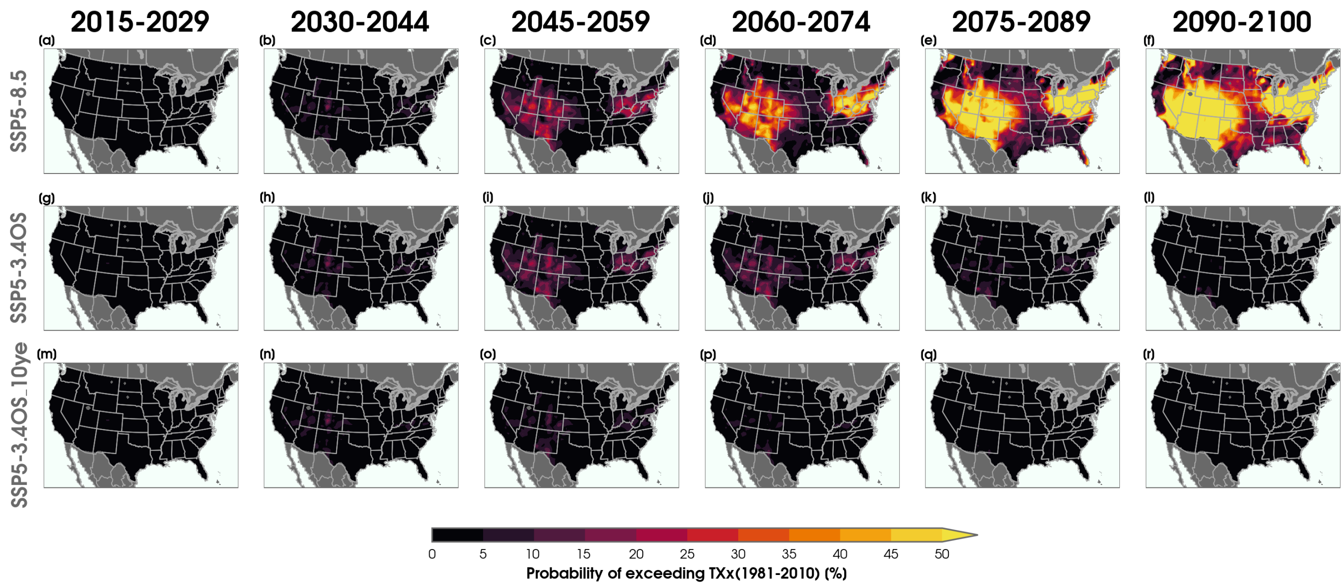


Figure 6: (a) Probability of a month having at least one day that exceeds the historical JJA highest daily maximum temperature (TXx) for SSP5-8.5 in 2015 to 2029, (b) 2030 to 2044, (c) 2045 to 2059, (d) 2060 to 2074, (e) 2075 to 2089, and (f) 2090 to 2100. (g-l) Same as (a-f), but for SSP5-3.4OS. (m-r) Same as (a-f), but for SSP5-3.4OS_10ye. Note that the data for the years from 2015 to 2030 are taken from SSP5-3.4OS in this third row. The historical TXx threshold is calculated separately at each grid point over the 1981 to 2010 reference period by considering all ensembles in the historical scenario and across all days in the months of JJA. The probabilities are further calculated by using all ensemble members and months per each epoch for the respective climate scenarios.

Similar reductions are found in Figure S6 for the frequency of intense minimum temperatures (TNx) when looking at SSP5-3.4OS_10ye compared to SSP5-3.4OS. However, the spatial pattern is quite different relative to TXx. For nighttime temperatures, the highest probability of exceeding the historical TNx is instead found over Florida followed by the northwestern half of CONUS, Southeast Gulf Coast, and in the Northeast. Again, this risk is much higher when following the extreme SSP5-8.5 scenario, with up to a 94% probability in 2090-2100.

### *3.3. Benefits of Earlier Climate Mitigation*

Rather than concentrate just on the reversibility and nonlinearity of changes in summertime heat extremes, as previously discussed, our focus now moves toward more closely comparing the regional differences between SSP5-3.4OS and SSP5-3.4OS_10ye. So far, our results suggest that even waiting to start mitigation efforts as little as 10 years later can broadly lead to more intense daytime and nighttime heat extremes across the CONUS throughout the remainder of the 21st century and beyond. Thus, in order to better understand the added value of the timing of reducing greenhouse gases on regional temperature extremes, we create a simple metric and denote this as an added climate 'benefit.' In other words, the word benefit is used here to suggest that there are fewer hot days and thus likely reduced heat stress impacts on society and ecosystems. These results are shown in Figure 7. A caveat is that we focus on the forced response differences for assessing mean climate benefits, and the exact values in reality would differ depending on the realization of internal variability.

To summarize this calculation, we first estimate the number of Tx90 days at each individual grid point across the CONUS for SSP5-3.4OS and SSP5-3.4OS_10ye. We then identify the year of the maximum number of Tx90 days in the ensemble mean of SSP5-3.4OS_10ye. Next, we identify the first year that the number of Tx90 days in the ensemble mean of SSP5-3.4OS falls below this peak and calculate the difference between these two time periods. To reveal simplified cost-benefit climate impacts, we then subtract 10 years from this difference estimate given that mitigation efforts in SSP5-3.4OS start approximately one decade later than SSP5-3.4OS_10ye. These results are displayed for each grid point in Figure 7a, where we find many areas of the central and eastern CONUS that see an added net benefit of more than 5 to 15 years as a result of starting large-scale emission mitigations a decade sooner. In other words, for these regions with a net benefit between 5 and 15 years, delaying mitigation by 10 years results in heat extreme occurrences that exceed the no-delay peak for another 15 to 25 years before falling below that peak. We do acknowledge though that the fact of starting mitigation 10 years earlier in the SSP5-3.4OS_10ye simulation is arguably also a benefit, which is not part of the explicit calculation shown here in Figure 7a-c.

A demonstration of this approach is shown in Figure 7d for an arbitrarily selected grid point in central Indiana. For this location, there are 26 years between the maximum count of Tx90 days in SSP5-3.4OS_10ye from until the ensemble mean of SSP5-3.4OS reaches this same value. This yields a benefit of 16 years by starting the earlier mitigation. As expected, however, there is significant interannual variability even in the ensemble mean, which impact our results on this estimate. We then adjust the definition of the metric to better account for this variability by applying two different techniques. In the first approach, we include a caveat that the ensemble mean of Tx90 for SSP5-3.4OS must stay below the maximum from SSP5-3.4OS_10ye for at least 10 consecutive years (Figure 7b). In the second approach, we instead apply a 10-year smoothing filter to the time series of each overshoot scenario's ensemble mean and then proceed by calculating the same differences in years as before (Figure 7c). Unsurprisingly, we find greater net benefits across the United States since these definitions attempt to further isolate the forced response from the effects of interannual to decadal variability. Examples of these two exercises are shown in Figure 7d and 7e for the same location in central Indiana. Note that the raw values for the differences in years between SSP5-3.4OS and SSP5-3.4OS_10ye (i.e., without subtracting a decade) are provided in Figure

S7a-c. Lastly, there are a few locations without any benefit that are masked in grey. Recall that for this benefit calculation we only consider the maximum count of Tx90 days after mitigation efforts are well underway in the overshoot scenarios. Consequently, there are a smaller number of locations with the maximum in Tx90 before this period of time; an example of this artifact is demonstrated in Figure S7d-e for a randomly selected location in western Minnesota.

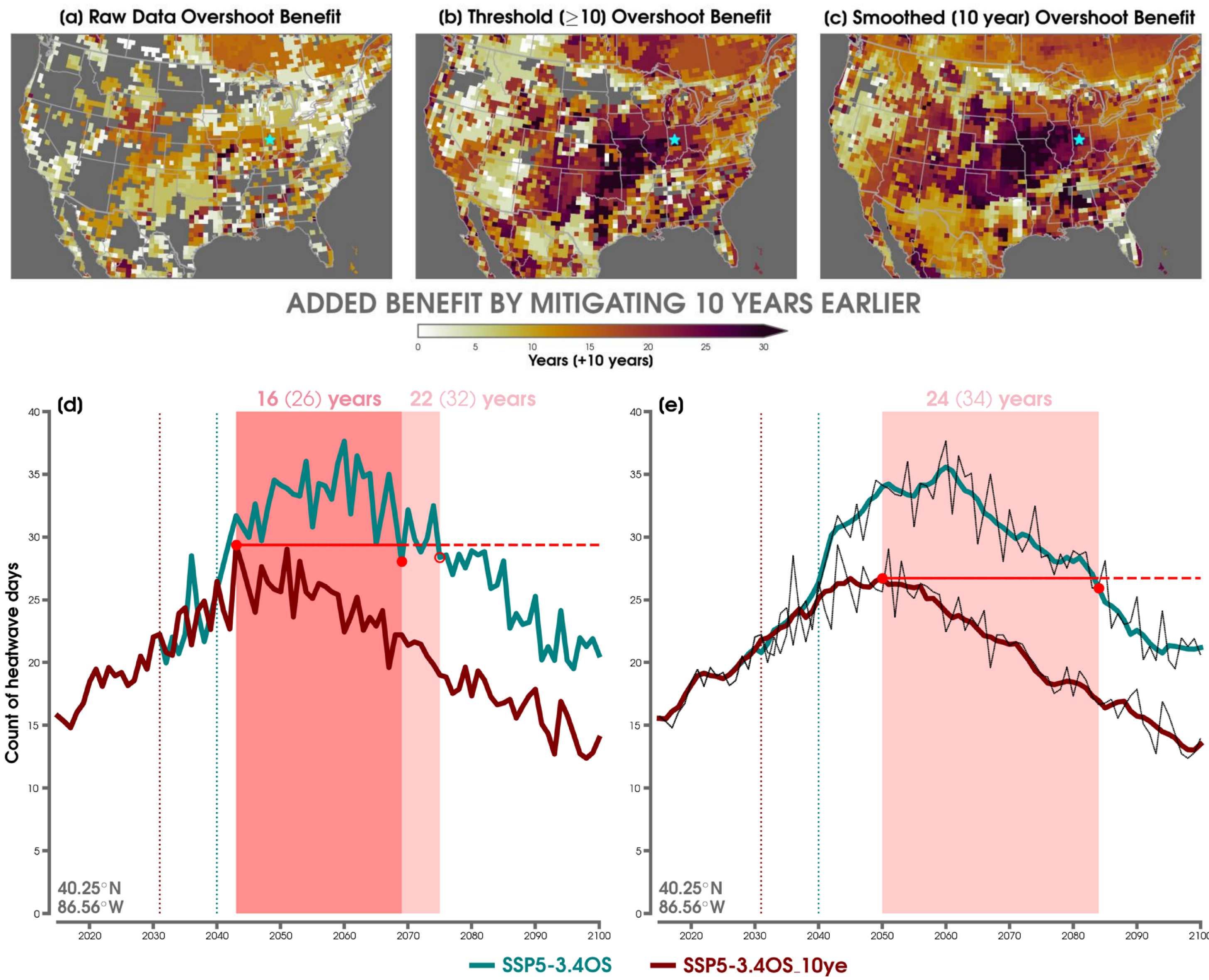
(a) Raw Data Overshoot Benefit
(b) Threshold (≥10) Overshoot Benefit
(c) Smoothed (10 year) Overshoot Benefit
ADDED BENEFIT BY MITIGATING 10 YEARS EARLIER
0 5 10 15 20 25 30
Years (+10 years)
(d)
16 (26) years
22 (32) years
Count of heatwave days
40.25°N
86.56°W
(e)
24 (34) years
40.25°N
86.56°W
SSP5-3.4OS
SSP5-3.4OS_10ye

Figure 7: (a) Map of the differences in years between when the maximum number of Tx90 summer days is reached for the ensemble mean of SSP5-3.4OS_10ye compared to the year that the ensemble mean of SSP5-3.4OS first falls below this maximum after its peak in $CO_2$ concentrations. This is calculated at each grid point. 10 years is subtracted off this difference value at each location to highlight the added benefit by mitigating 10 years earlier (see text; "+10 years"). Grid points with a raw difference of less than 10 years are masked out in gray. A blue star highlights the location of the example in (d-e). (b) Same as (a), but for the first year in SSP5-3.4OS when at least the next 10 years remain consistently below this maximum number of Tx90 days in SSP5-3.4OS_10ye. (c) Same as (a), but after applying a Savitzky-Golay filter (Savitzky and Golay, 1964) with a 10-year smoothing window (3rd order polynomial) to the ensemble mean count of Tx90 at each grid point and for each respective climate scenario. (d) An example of this methodology for a location in central Indiana (approximately 40.25°N and 86.56°W) showing the time series of the count of Tx90 summer days in SSP5-3.4OS_10ye (dark red line) and SSP5-3.4OS (dark green line) from 2015 to 2100. The red solid circle on the SSP5-3.4OS_10ye time series indicates the maximum count of Tx90 at this location for the ensemble mean. The red solid circle on the SSP5-3.4OS time series highlights the first year that the ensemble mean count of Tx90 at this location falls below the SSP5-3.4OS_10ye maximum. The darker red shading shows the difference in years between these two points (26 years, where $26 - 10 = 16$ years) which is shown in the approach for map (a). A horizontal solid red line is added to annotate the width of this red shading. The open red circle on the SSP5-3.4OS is the year where the proceeding 10 years remain less than the SSP5-3.4OS_10ye Tx90 maximum (illustrated by the horizontal dashed red line). The lighter red shading shows the difference in years between these two points (32 years, where $32 - 10 = 22$ years) which is shown in the approach for map (b). Dashed vertical lines are shown for the start of climate mitigation in SSP5-3.4OS_10ye (dark red) and SSP5-3.4OS (dark green). (e) Same as (d), but after applying the Savitzky-Golay filter to the time series of SSP5-3.4OS_10ye (dark red line) and SSP5-3.4OS_10ye (dark green line). The raw data for each climate scenario from panel (d) is also shown with a thin dashed black line. The light red shading annotates the difference in years between these two points (34 years, where $34-10 = 24$ years) which is shown in the approach for map (c) along with added illustrations of the solid and dashed horizontal red lines.

Despite the various differences in the technical details across Figures 7 and S7, a clear theme emerges in these SPEAR simulations — earlier mitigation reduces the number of years with higher Tx90 summertime days for a length of time that exceeds the difference between onset times of mitigation. To put it another way, an earlier rapid reduction in greenhouse gases leads to an even greater decrease in overall impacts related to the frequency of CONUS heat extremes. In fact, for some portions of the central United States, it can take up to 30 years before the number of Tx90 days in SSP5-3.4OS falls below the peak simulated by SSP5-3.4OS_10ye (Figure 7a-c). One possible interpretation of this regional pattern is that the response to changes in external forcing in the central United States could be slower or weaker than in other regions (e.g., it takes longer to see the difference between SSP5-3.4OS_10ye and SSP5-3.4OS). Moreover, this region in the central Great Plains is a hotspot for strong land-atmosphere coupling (Koster et al., 2004), which could also influence the persistence of heatwave days in the future.

### *3.4. Mechanisms Associated with Mean Changes After Mitigation*

We next investigate the possible drivers responsible for the added benefit of earlier mitigation, including the spatial heterogeneity of this measure, by examining changes in other large-scale climate fields within the SPEAR overshoot scenarios. Figure 8 shows the global response of T2M for a GWL of 1.7°C for a composite from SSP5-8.5 relative to after-peak warming in the overshoot scenarios. In response to the elevated levels of greenhouse gas forcing relative to the 1921-1950 reference period, we see a characteristic global warming fingerprint across the globe (Figure 8a-c), accompanied by larger anomalies over land areas and in the polar regions (Manabe and Stouffer, 1980). However, a stronger North Atlantic warming hole signature is visible in the composites of the overshoot scenarios (Figure 8b-c) compared to SSP5-8.5 (Figure 8a). Although this temperature pattern is found in real-world observations as well as GCM simulations, it remains uncertain whether this feature in nature is driven by internal variability or external forcing (e.g., Drijfhout et al., 2012; Chemke et al., 2020; Dagan et al., 2020; Keil et al., 2020; Menary et al., 2020; He et al., 2022), such as through the response to a weakening in the strength of the AMOC (Bellomo et al., 2021).

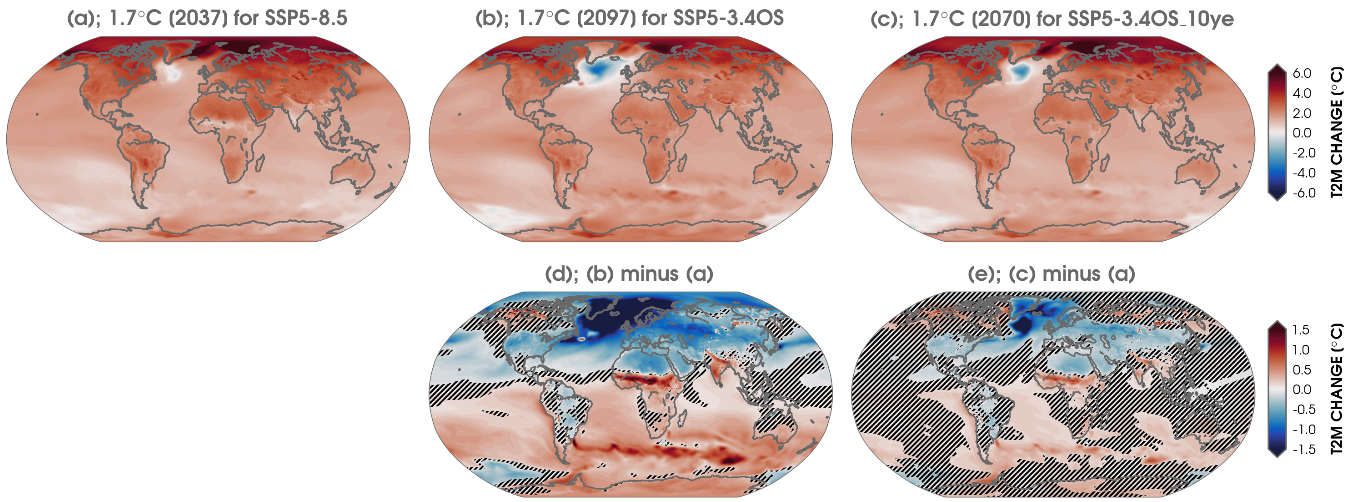


Figure 8: Same as Figure 4, but for global composites of near-surface air temperature (T2M) change.

In a similar approach to the earlier GWL analysis of heat extremes (i.e., Figure 4), we subsequently show the differences in the composites at 1.7°C to understand the potential reversibility of the seasonal mean T2M response for SSP5-3.4OS (Figure 8d) and SSP5-3.4OS_10ye (Figure 8e). A hemispheric-scale dipole is found in the temperature difference pattern with greater warming across the Southern Hemisphere and more cooling across the Northern Hemisphere for the same GWL during the drawdown in greenhouse gas concentrations. Strong, statistically significant cooling of several degrees is shown across the North Atlantic and Arctic, particularly for SSP5-3.4OS (Figure 8d). This cooling signature is consistent with a persistent weakening of AMOC that is simulated by SPEAR and found across all future climate scenarios despite their differences in radiative forcing later in the 21st century (see Figure 3 in Delworth et al., 2022). An analogous view of sea surface temperature (SST) differences is also displayed in Figure S8, and the same general pattern and magnitude of response is found when compared to T2M. While the largest cooling is evident over the far north Atlantic Ocean south of Iceland, T2M differences cooler than -1.5°C extend into western Europe across Scandinavia in SSP5-3.4OS. Recent analysis from Pfleiderer et al. (2024) has identified substantial inter-model spread across CMIP6 simulations with SSP5-3.4OS forcing, but there are at least a few other GCMs (e.g., CESM2-WACCM) that have a similar AMOC decline and thus resulting evolution of temperature anomalies by hemisphere. Other interesting features in Figure 8d-e include enhanced warming over the Southern Ocean and across portions of Central Africa and India, where the latter is likely related to a modulation of the intertropical convergence zone (ITCZ) (Moreno-Chamarro et al., 2020). Aligned with the earlier results of enhanced reductions in JJA heat extreme days across CONUS, we see cooling in average T2M over these same areas too (Figure 8d-e). Slightly less cooling is found in the differences of T2M for SSP5-

3.4OS_10ye at a GWL of 1.7°C (Figure 8e). It is conceivable that this is related to the earlier and smaller peak in radiative forcing and consequently leading to an earlier stabilization and recovery of the AMOC, as pointed out by Delworth et al. (2022) for SSP1-1.9 using the same SPEAR model.

Figure 9 more closely compares the differences in the mean temperature response of each hemisphere to SSP5-8.5, SSP5-3.4OS, and SSP5-3.4OS_10ye forcing in JJA. The timing of peak ensemble-mean warming in the Northern Hemisphere for the overshoot runs is reached close to the year of the annual-mean maximum GMST and begins to steadily decline thereafter (Figure 9a). However, for the Southern Hemisphere, ensemble mean T2M decreases at a much slower rate and only declines by 0.36°C through 2100 for SSP5-3.4OS and 0.54°C for SSP5-3.4OS_10ye compared with their temperature peaks. This is compared to mean declines in the Northern Hemisphere of 0.97°C and 1.11°C for SSP5-3.4OS and SSP5-3.4OS_10ye, respectively.

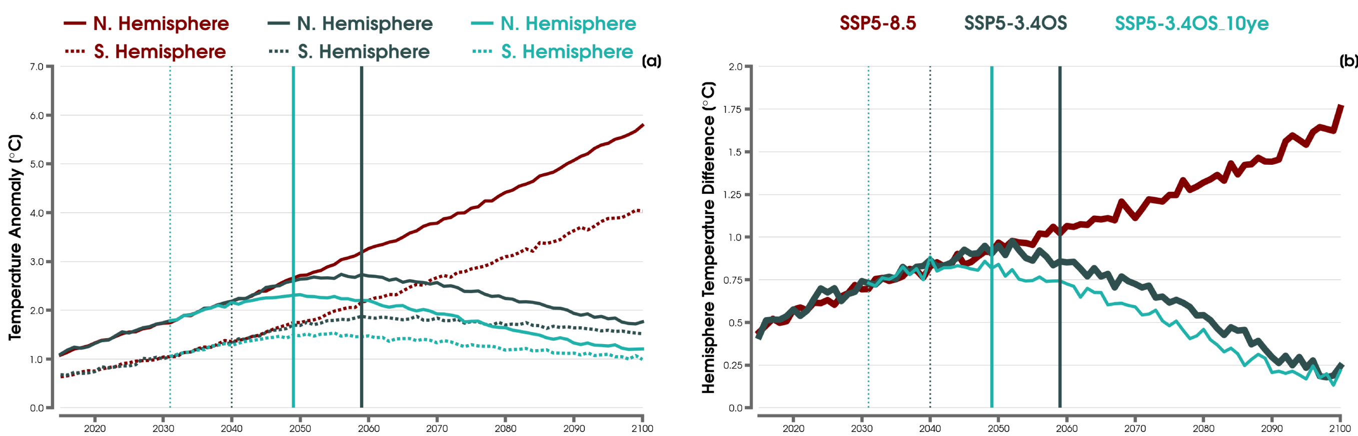


Figure 9: (a) Time series of mean JJA temperature anomalies averaged over the Northern Hemisphere from 2015 to 2100 for the SPEAR ensemble mean following SSP5-8.5 from 2015 to 2100 (solid red line), SSP5-3.4OS from 2015 to 2100 (solid dark green line), and SSP5-3.4OS_10ye from 2031 to 2100 (solid light green line). The mean temperature anomalies averaged for the Southern Hemisphere are shown with dashed lines in their same colors corresponding to each climate scenario. Anomalies are computed with respect to their 1921-1950 climatological time means. The dashed vertical lines indicate the start of climate mitigation in 2031 (light green) and 2040 (dark green) for SSP5-3.4OS_10ye and SSP5-3.4OS, respectively. The solid vertical lines indicate the maximum ensemble-mean GMST for SSP5-3.4OS_10ye (light green) and SSP5-3.4OS (dark green), respectively. (b) Time series of the difference in the mean JJA Northern Hemisphere temperature anomaly minus the mean JJA Southern Hemisphere temperature anomaly shown in solid lines with the same colors for each climate scenario.

The divergence in the rate of change in hemispheric mean T2M anomalies is more clearly depicted in Figure 9b. Here we find a significant difference in the temperature contrast between the Northern and Southern Hemispheres. Unlike under steadily rising radiative forcing that corresponds to a widening contrast between the two hemispheres (Manabe et al., 1992; Friedman et al., 2013; Zhang et al., 2024), we instead see a reduced temperature asymmetry in response to aggressive climate mitigation efforts. In fact, the temperature anomaly contrast drops to between 0.2 to 0.25°C by the year 2100 in the overshoot scenarios, which is substantially smaller than even the start of the future projections in 2015 (0.4°C). This result again supports that even though the average GMST is cooling, there are clear distinctions in the reversibility of regional climate patterns that are likely modulated by differences in the response of the land surface and through ocean heat transport.

Previous work has highlighted that land-atmosphere-ocean coupling, including processes related to surface vegetation and relative humidity from moisture transport between the land and ocean (Joshi and Gregory, 2008; Joshi et al., 2008; Byrne and O'Gorman, 2013; Byrne and O'Gorman, 2018; Zarakas et al., 2020), can be considered by looking at changes in a simple metric called the land-sea warming ratio (Sutton et al., 2007). Figure S9 shows this diagnostic, which is computed here for JJA as the global mean T2M over land areas divided by the global mean SST. For the SSP5-8.5 ensemble mean, the land-sea warming ratio is rather steady around 1.78, though with less variability as radiative forcing accelerates later in the 21st century. This value aligns with the large spread found across observations and earlier generations of CMIP coupled models (Sutton et al., 2007; Wallace and Joshi, 2018; IPCC, 2023c). Yet, a stark contrast begins to emerge by 2060 for the overshoot experiments. Under both SSP5-3.4OS and SSP5-3.4OS_10ye, we see a consistent decline in the land-sea warming ratio through 2100. The warming ratio reaches 1.63 for SSP5-3.4OS and 1.59 for SSP5-3.4OS_10ye, which is a result of the land cooling faster than the ocean surface during the last few decades of the 21st century. The broader implication here is that a decrease in the land-sea temperature gradient could play a role in modulating CONUS heat extremes through changes in heat and moisture advection (Holmes et al., 2016; Horton et al., 2016), especially at regional scales (Barriopedro et al., 2023).

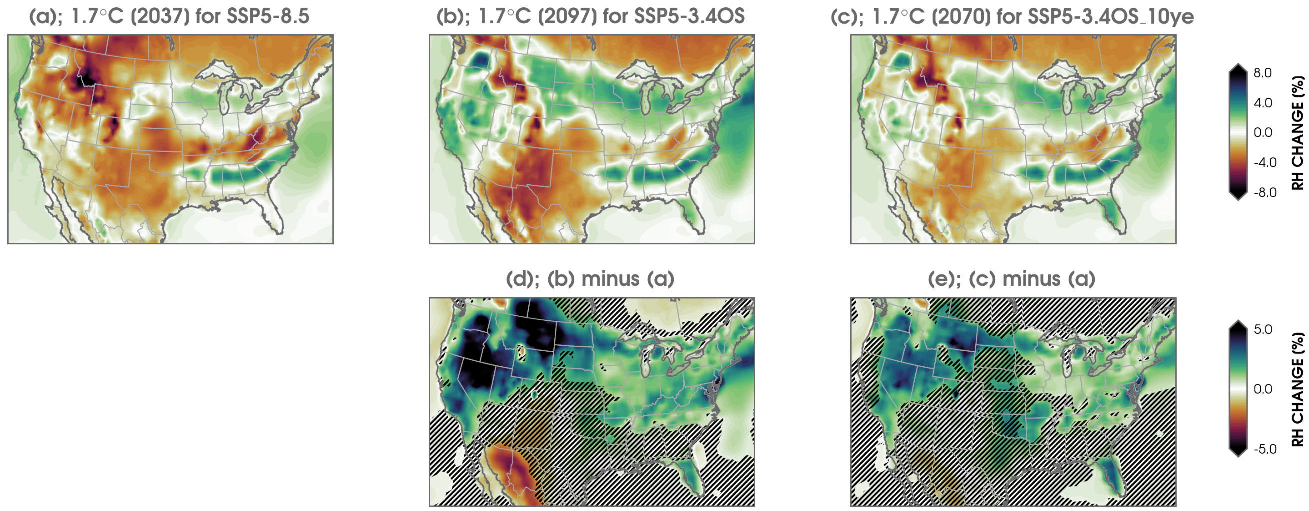


Figure 10: Same as Figure 4, but for composites of near-surface relative humidity (RH) change.

Given the theorized connections between the land-sea contrast, humidity, and land surface air temperature (e.g., Byrne and O'Gorman, 2013), we next examine changes in relative humidity over the CONUS as a function of GWL of 1.7°C using the SSP5-8.5, SSP5-3.4OS, and SSP5-3.4OS_10ye scenarios (Figure 10). In response to radiative forcing, decreases in near-surface relative humidity are found across the western United States (Figure 10a), and this is consistent with previous work for observed and modeled trends (Pierce et al., 2013; Dunn et al., 2017; Vicente-Serrano et al., 2018). While most land areas show decreases in humidity (Figure 10a), two bands of increases in relative humidity are found across the eastern half of the CONUS, including over the minimum in Tx90 change over the Southeast. However, this highly regionally-dependent response may again relate to a modeled sensitivity of land-atmosphere interactions and land surface change (Berg et al., 2016; Findell et al., 2017). Nevertheless, for the overshoot simulations, we find statistically significant increases in humidity across most of CONUS when comparing the composite differences for after climate mitigation relative to before at equivalent GWLs of 1.7°C (Figure 10d-e). These differences are particularly largest (more than 5% higher relative humidity) across the higher elevations of the western United States and in the vicinity of the larger reductions in heat extremes when comparing with Figure 4.

Coinciding with the comparative increases in near-surface humidity at the same GWL for SSP5-3.4OS and SSP5-3.4OS_10ye is an increase in ensemble mean precipitation for the CONUS-wide average in JJA (Figure 11). This is distinct from the decreases in ensemble mean precipitation simulated under SSP5-8.5, though a relatively flat trend is found for SSP2-4.5 through 2100. Figure S10 shows a global view of the change in precipitation in JJA at GWLs of 1.7°C for SSP5-8.5 and the two overshoot simulations. In agreement with the area-wide average in Figure 11, there are relative increases in precipitation that are statistically significant particularly for the northwestern portion of CONUS (Figure S10d-e). In addition, zooming out from CONUS, we see a significant modulation of the ITCZ that is likely linked to changes in the strength of AMOC in these model experiments (Moreno-Chamarro et al., 2020; Delworth et al., 2022).

Given the tight coupling between seasonal-mean precipitation and summertime temperatures in CONUS (Huang and Dool, 1993; Eischeid et al., 2023; Schreck et al., 2024), the relative increases in rainfall and surface humidity can be linked to the greater reductions in Tx90 days for the overshoot scenarios. These set of mechanisms describe the role for a positive feedback loop-like effect. Figure S11 briefly addresses the connection to the large-scale circulation response by looking at geopotential height changes at 500 hPa. As expected in response to external radiative forcing (Christidis and Stott, 2015; He et al., 2024), a thermally-driven increase in the height of the troposphere is found across the globe (Figure S11a-c). Despite this warming, a hemispheric dipole structure is again found for the differences in Z500 anomalies when comparing composites before and after peak greenhouse concentrations in the overshoot experiments (Figure S11d-e). Here a reduction in Z500 is found over the Northern Hemisphere with a maximum difference stretching across the North Pacific and into the western United States. This spatial pattern is found when comparing both SSP5-3.4OS (Figure S11d) and SSP5-3.4OS_10ye (Figure S11e). While this may simply coincide with a thermodynamic fingerprint, as found in the surface temperature response pattern in Figure 8, it is interesting to note that some of the largest height reductions accompany the greatest reductions in heat extremes and heavier mean rainfall. This suggests the potential role for an increase in low pressure and implied cloudiness over the western half of CONUS in relation to the dampening of maximum summertime heat. The overall atmospheric circulation response to the timing of rapid drawdowns in greenhouse gases is worth more investigation in future work.

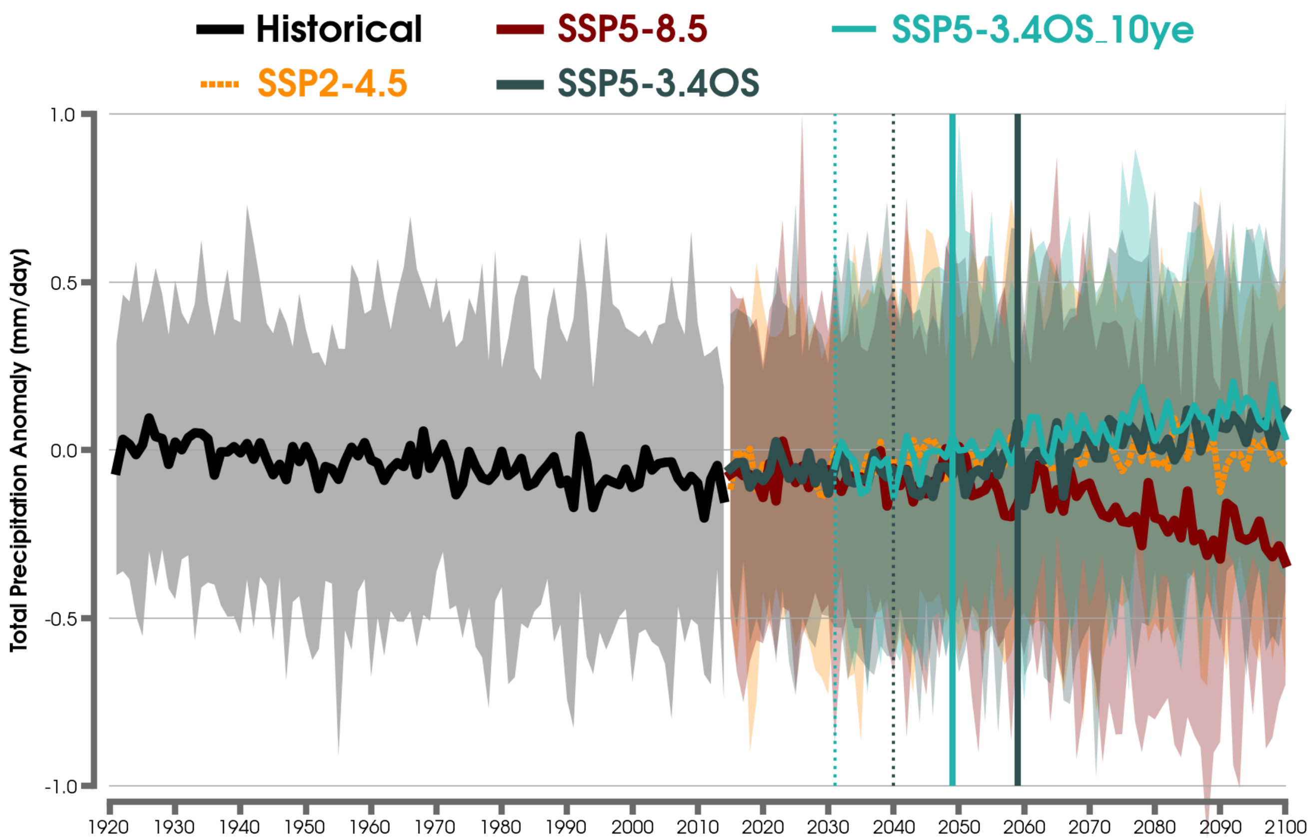


Figure 11: Time series of mean JJA precipitation anomalies averaged for the CONUS from 1921 to 2100 for the ensemble mean of SPEAR following the historical climate scenario from 1921 to 2014 (solid black line) and the same future climate scenarios from Figure 1. The spread across ensemble members is shown with the lighter shading for each respective experiment. Anomalies are computed with respect to the 1921-1950 climatological time mean. The dashed vertical lines indicate the start of climate mitigation in 2031 (light green) and 2040 (dark green) for SSP5-3.4OS_10ye and SSP5-3.4OS, respectively. The solid vertical lines indicate the maximum ensemble-mean GMST for SSP5-3.4OS_10ye (light green) and SSP5-3.4OS (dark green), respectively.

Figure 12 summarizes the sensitivity of average CONUS Tx90 days to mean precipitation, surface evaporation, and near-surface relative humidity anomalies in the SPEAR Large Ensemble under SSP5-3.4OS and SSP5-8.5 scenarios. Previous studies have considered similar types of framing for identifying different characteristics of heatwaves that can be classified, for instance, according to moisture availability and/or land surface processes (Rastogi et al., 2020; Thomas et al., 2020; Barriopedro et al., 2023; Tian, Kleidon, Lesk, Zhou, Luo, Ghausi, Wang, Zhong and Zscheischler, 2024). We also evaluate whether these relationships change over different 15-year epochs; this includes prior to the start of mitigation efforts for the overshoot experiments, the period following the respective peak count in Tx90 days for SSP5-3.4OS, and the period of 2086 to 2100 that is common to all scenarios. A parallel version of this figure is shown in Figure S12 for SSP5-3.4OS_10ye with quantitatively similar results found. Weaker, but significant negative correlations are also found for relationships with Tn90 (not shown). While these spatially-integrated diagnostics neglect the role of regional-scale variations in revealing local heatwave drivers that can exist across the CONUS (Smith et al., 2013; Benson and Dirmeyer, 2021; Yoon et al., 2024), it still provides a conditional attribution-like overview as to the relationships between dryness and extreme heat under different radiative forcing scenarios.

Here, changes in seasonal mean precipitation, evaporation, and humidity are significantly negatively correlated with the number of JJA heat extreme days averaged across CONUS. Regression slope coefficients remain nearly constant despite differences in external forcing, including when the background mean warming in SSP5-8.5 shifts the distribution to the right with an increase in the number of Tx90 days (Figure 12). The tendency for an increase in precipitation and overall moisture availability, such as through wetter soils and suppressed sensible heat fluxes (Koster et al., 2003; Miralles et al., 2019), contributes to the dampening of heat extreme day frequency after peak radiative forcing in the overshoot scenarios. This coupling is also evident by comparing the shift of the joint distribution from the 2025-2039 (green dots) to the 2086-2100 (orange dots) period. Recent studies of observational trends of heatwaves across CONUS further support these findings found in SPEAR for connecting precipitation anomalies to daytime extreme temperatures (e.g., Yang et al., 2019; Thomas et al., 2020), which is typically physically expressed through departures in cloud cover, soil moisture, and surface energy fluxes.

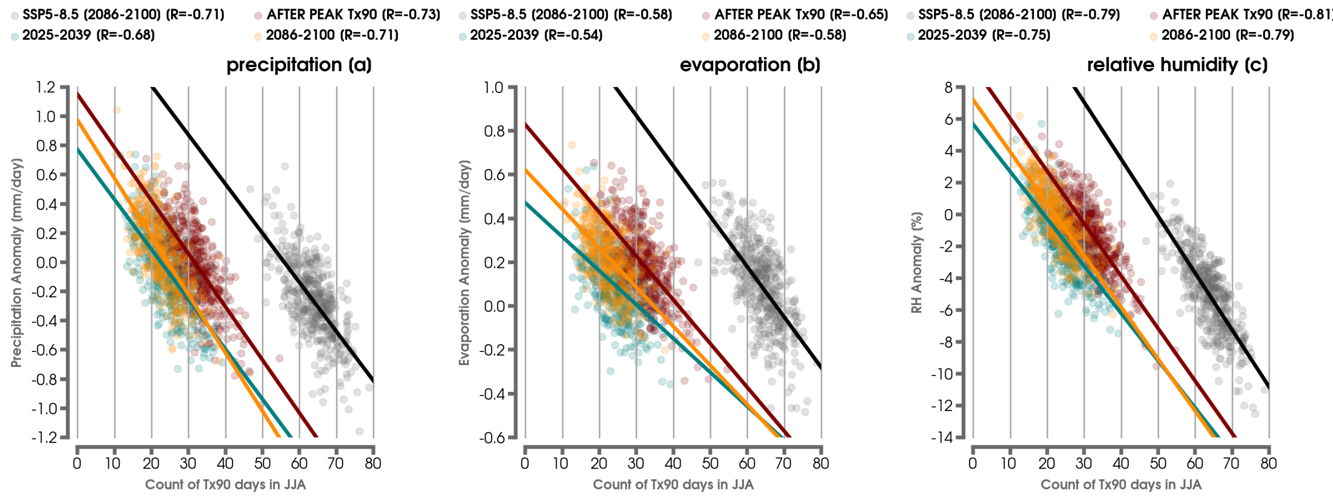


Figure 12: (a) The relationship of changes in mean precipitation relative to the number of Tx90 days in JJA averaged across CONUS for SSP5-8.5 in 2086 to 2100 (gray dots). This relationship is also shown for SSP5-3.4OS in years 2025 to 2039 (blue dots), the 15 years after the ensemble mean's highest count of Tx90 days in SSP5-3.4OS (orange dots), and for the 2086 to 2100 period in SSP5-3.4OS (dark red dots). Anomalies are computed with respect to the 1921 to 1950 climatological mean. The scatter points consider all years and ensemble members for each epoch period. A solid line is displayed for the linear least squares fit along with its corresponding Pearson correlation coefficient (R) listed in the legend. (b) Same as (a), but for Tx days related to changes in mean evaporation, (c) Same as (a), but for Tx days related to changes in mean relative humidity. All correlations are statistically significant at $p < 0.01$.

## 4. Summary and Conclusions

Given the widespread societal and environmental impacts associated with recent historical heatwave events in the United States and the projected increases moving forward into the near-term (Anderson and Bell, 2011; Horton et al., 2016; Breshears et al., 2021; Rogers et al., 2021; Domeisen et al., 2023), it is crucial to better understand their characteristics to a wider range of possible realizations of the future. For improving decision-making and planning purposes, this includes accounting for scenarios of both increasing or decreasing radiative forcing (Nature, 2023), since climate impacts may not always be straightforward even after carbon reductions. This study therefore examined the potential reversibility of heat extreme days across the conterminous United States in response to two scenarios that simulate rapid climate mitigation efforts but differ in the start of their implementation by approximately a decade (SSP5-3.4OS and SSP5-3.4OS_10ye). We also compared these overshoot scenarios with standard climate change pathways associated with increasing radiative forcing. These future scenarios were examined through the lens of the GFDL SPEAR Large Ensemble (Delworth et al., 2020), which is a fully-coupled climate model that includes a relatively high spatial resolution and 30 ensemble members in each simulation in each simulation; the combination of large ensemble size and horizontal resolution provides benefits for quantifying the role of internal variability and for simulating extreme events in future projections. A particular emphasis of this study is to outline a simplified cost-benefit-like framing (i.e., shortened years with heat exposure) for looking at variations in the maximum number of heat extreme days at the local scale depending on the timing of significant reductions in greenhouse gas emissions.

Our results imply a notable benefit in terms of reduced extreme heat days across large portions of the CONUS in response to decreasing radiative forcing from hypothetical climate mitigation efforts. There are even greater heat risk reductions by starting the curtailment of fossil fuel emissions in as little as one decade sooner than later, as simulated by the SPEAR model. Quantitatively similar changes are found for both anomalously warm daytime and nighttime temperatures. The smaller relative number of summer heat extreme days at equivalent levels of global warming after peak emissions compared to before peak is broadly linked here to a faster rate of mean thermodynamic cooling over land areas relative to the ocean in the northern extratropics. This dampening of heat extreme frequency over CONUS is further associated with an enhancement of the hydrologic cycle that includes greater relative precipitation and surface humidity during summer, especially across the inner mountain West. Changes in the hemispheric temperature anomaly dipole are also found after radiative forcing starts declining, which aligns with Delworth et al. (2022) in suggesting an important role for the strength of the AMOC continuing to drive a large-scale mean response and influencing the potential for climate irreversibility of some phenomenon.

Moving forward, it will be important to compare these results by conducting similar types of overshoot experiments in other GCMs, especially those with a large number of ensemble members that can be used to adequately consider the role of internal variability (Tebaldi and Friedlingstein, 2013; Diffenbaugh et al., 2023). The rate of greenhouse gas drawdown could also play a crucial role in the large-scale climate response and should be further interested in future work. Even though the implications of our results are limited due to potential biases by the SPEAR model, at least several other GCMs in CMIP6 were found to have a similar surface temperature evolution in the SSP5-3.4OS scenario after peak emissions (Pfleiderer et al., 2024). Further research and model development is also needed to refine projections of the sensitivity of the AMOC to future changes in radiative forcing (Roberts et al., 2020; Weijer et al., 2020; Bellomo et al., 2021), given that it could have an important role in the hysteresis and reversibility of regional climate impacts like through temperature extremes. To credibly address all potential hazard risks and benefits for developing regional climate services, our results argue that overshoot pathways should be regularly developed and analyzed as part of the standard portfolio of future scenarios.

## Conflict of interest

The authors declare no conflicts of interest.

## Data Availability Statement

The data that support the findings of this study are available at the following URL: `https://www.gfdl.noaa.gov/spear_large_ensembles/` using the GFDL data portal and additional data for temperature and precipitation with other climate scenarios can be found at `https://zenodo.org/records/10727521`. The SPEAR Large Ensemble is more broadly discussed in Delworth et al. (2020).

This study primarily uses Python v3.9.13 (Rossum and Drake, 2009) under the Conda v23.1.0 (Anaconda, 2023) distribution system. Individual Python packages that were applied also include Numpy v1.22.4 (Harris et al., 2020), Scikit-learn v1.1.1 (Pedregosa et al., 2011), SciPy v1.8.1 (Virtanen et al., 2020), Matplotlib v3.5.2 (Hunter, 2007), Basemap v1.3.6, (*Basemap*, 2022), cmocean v2.0 (Thyng et al., 2016), and CMasher v1.6.3 (van der Velden, 2020). Some processing of the SPEAR large ensemble data was also done using CDO v1.9.10 (Schulzweida, 2019) and NCO v5.0.1 (Zender, 2008).

## Acknowledgments

We thank Dr. Weixuan Xu and Dr. Donghyuck Yoon for their insightful comments and suggestions on the GFDL internal review of the essay. This article was prepared by Zachary M. Labe under CIMES award NA23OAR4320198 from NOAA, U.S. Department of Commerce, as well as support from the Climate Program Office and base funding of GFDL provided by NOAA. The statements, findings, conclusions, and recommendations are those of the authors and do not necessarily reflect the views of NOAA, or the U.S. Department of Commerce.

## References

Abatzoglou, J. T. and Barbero, R. (2014). Observed and projected changes in absolute temperature records across the contiguous united states, *Geophysical Research Letters* **41**.

Adcroft, A., Anderson, W., Balaji, V., Blanton, C., Bushuk, M., Dufour, C. O., Dunne, J. P., Griffies, S. M., Hallberg, R., Harrison, M. J., Held, I. M., Jansen, M. F., John, J. G., Krasting, J. P., Langenhorst, A. R., Legg, S., Liang, Z., McHugh, C., Radhakrishnan, A., Reichl, B. G., Rosati, T., Samuels, B. L., Shao, A., Stouffer, R., Winton, M., Wittenberg, A. T., Xiang, B., Zadeh, N. and Zhang, R. (2019). The gfdl global ocean and sea ice model om4.0: Model description and simulation features, *Journal of Advances in Modeling Earth Systems* **11**: 3167–3211.
**URL:** *https://agupubs.onlinelibrary.wiley.com/doi/10.1029/2019MS001726*

Amengual, A., Homar, V., Romero, R., Brooks, H. E., Ramis, C., Gordaliza, M. and Alonso, S. (2014). Projections of heat waves with high impact on human health in europe, *Global and Planetary Change* **119**.

Amnuaylojaroen, T., Parasin, N. and Limsakul, A. (2024). Projections and patterns of heat-related mortality impacts from climate change in southeast asia, *Environmental Research Communications* **6**.

Anaconda (2023). Conda (version 23.1.0) [software].
**URL:** *https://github.com/conda/conda/tree/main https://docs.conda.io/projects/conda/en/23.1.x/index.html*

Anderson, G. B. and Bell, M. L. (2011). Heat waves in the united states: Mortality risk during heat waves and effect modification by heat wave characteristics in 43 u.s. communities, *Environmental Health Perspectives* **119**.

Banerjee, A., Polvani, L. M. and Fyfe, J. C. (2017). The united states "warming hole": Quantifying the forced aerosol response given large internal variability, *Geophysical Research Letters* **44**.

Barriopedro, D., García-Herrera, R., Ordóñez, C., Miralles, D. G. and Salcedo-Sanz, S. (2023). Heat waves: Physical understanding and scientific challenges, *Reviews of Geophysics* **61**.

*Basemap* (2022).
**URL:** *https://github.com/matplotlib/basemap*

Bellomo, K., Angeloni, M., Corti, S. and von Hardenberg, J. (2021). Future climate change shaped by inter-model differences in atlantic meridional overturning circulation response, *Nature Communications* **12**.

Benjamini, Y. and Hochberg, Y. (1995). Controlling the false discovery rate: A practical and powerful approach to multiple testing, *Journal of the Royal Statistical Society: Series B (Methodological)* **57**.

Benson, D. O. and Dirmeyer, P. A. (2021). Characterizing the relationship between temperature and soil moisture extremes and their role in the exacerbation of heat waves over the contiguous united states, *Journal of Climate* **34**.

Berg, A., Findell, K., Lintner, B., Giannini, A., Seneviratne, S. I., Hurk, B. V. D., Lorenz, R., Pitman, A., Hagemann, S., Meier, A., Cheruy, F., Ducharne, A., Malyshev, S. and Milly, P. C. (2016). Land-atmosphere feedbacks amplify aridity increase over land under global warming, *Nature Climate Change* **6**.

Blanusa, M. L., López-Zurita, C. J. and Rasp, S. (2023). Internal variability plays a dominant role in global climate projections of temperature and precipitation extremes, *Climate Dynamics* **61**.

Boeck, H. J. D., Dreesen, F. E., Janssens, I. A. and Nijs, I. (2010). Climatic characteristics of heat waves and their simulation in plant experiments, *Global Change Biology* **16**.

Boucher, O., Halloran, P. R., Burke, E. J., Doutriaux-Boucher, M., Jones, C. D., Lowe, J., Ringer, M. A., Robertson, E. and Wu, P. (2012). Reversibility in an earth system model in response to co2 concentration changes, *Environmental Research Letters* **7**.

Breshears, D. D., Fontaine, J. B., Ruthrof, K. X., Field, J. P., Feng, X., Burger, J. R., Law, D. J., Kala, J. and Hardy, G. E. J. (2021). Underappreciated plant vulnerabilities to heat waves, *New Phytologist* **231**.

Brown, S. J. (2020). Future changes in heatwave severity, duration and frequency due to climate change for the most populous cities, *Weather and Climate Extremes* **30**.

Byrne, M. P. and O'Gorman, P. A. (2013). Link between land-ocean warming contrast and surface relative humidities in simulations with coupled climate models, *Geophysical Research Letters* **40**.

Byrne, M. P. and O'Gorman, P. A. (2018). Trends in continental temperature and humidity directly linked to ocean warming, *Proceedings of the National Academy of Sciences of the United States of America* **115**.

Chemke, R., Zanna, L. and Polvani, L. M. (2020). Identifying a human signal in the north atlantic warming hole, *Nature Communications* **11**.

Chen, L. and Ford, T. W. (2021). Effects of 0.5c less global warming on climate extremes in the contiguous united states, *Climate Dynamics* **57**.

Christidis, N. and Stott, P. A. (2015). Changes in the geopotential height at 500 hpa under the influence of external climatic forcings, *Geophysical Research Letters* **42**.

Ciavarella, A., Stott, P. and Lowe, J. (2017). Early benefits of mitigation in risk of regional climate extremes, *Nature Climate Change* **7**.

Dagan, G., Stier, P. and Watson-Parris, D. (2020). Aerosol forcing masks and delays the formation of the north-atlantic warming hole by three decades, *Geophysical Research Letters* **47**.
**URL:** *https://agupubs.onlinelibrary.wiley.com/doi/full/10.1029/2020GL090778*

Delworth, T. L., Cooke, W. F., Adcroft, A., Bushuk, M., Chen, J.-H., Dunne, K. A., Ginoux, P., Gudgel, R., Hallberg, R. W., Harris, L., Harrison, M. J., Johnson, N., Kapnick, S. B., Lin, S.-J., Lu, F., Malyshev, S., Milly, P. C., Murakami, H., Naik, V., Pascale, S., Paynter, D., Rosati, A., Schwarzkopf, M., Shevliakova, E., Underwood, S., Wittenberg, A. T., Xiang, B., Yang, X., Zeng, F., Zhang, H., Zhang, L. and Zhao, M. (2020). Spear: The next generation gfdl modeling system for seasonal to multidecadal prediction and projection, *Journal of Advances in Modeling Earth Systems* **12**: e2019MS001895.
**URL:** *https://agupubs.onlinelibrary.wiley.com/doi/10.1029/2019MS001895*

Delworth, T. L., Cooke, W. F., Naik, V., Paynter, D. and Zhang, L. (2022). A weakened amoc may prolong greenhouse gas–induced mediterranean drying even with significant and rapid climate change mitigation, *Proceedings of the National Academy of Sciences of the United States of America* **119**: e2116655119.
**URL:** *https://www.pnas.org/doi/abs/10.1073/pnas.2116655119*

Deser, C., Lehner, F., Rodgers, K. B., Ault, T., Delworth, T. L., DiNezio, P. N., Fiore, A., Frankignoul, C., Fyfe, J. C., Horton, D. E., Kay, J. E., Knutti, R., Lovenduski, N. S., Marotzke, J., McKinnon, K. A., Minobe, S., Randerson, J., Screen, J. A., Simpson, I. R. and Ting, M. (2020). Insights from earth system model initial-condition large ensembles and future prospects, *Nature Climate Change* pp. 1–10.
**URL:** *http://www.nature.com/articles/s41558-020-0731-2*

Deser, C., Phillips, A., Bourdette, V. and Teng, H. (2012). Uncertainty in climate change projections: the role of internal variability, *Climate Dynamics* **38**: 527–546.
**URL:** *http://link.springer.com/10.1007/s00382-010-0977-x*

Diffenbaugh, N. S., Barnes, E. A. and Keys, P. W. (2023). Probability of continued local-scale warming and extreme events during and after decarbonization, *Environmental Research: Climate* **2**.

Domeisen, D. I., Eltahir, E. A., Fischer, E. M., Knutti, R., Perkins-Kirkpatrick, S. E., Schär, C., Seneviratne, S. I., Weisheimer, A. and Wernli, H. (2023). Prediction and projection of heatwaves.

Donat, M. G., King, A. D., Overpeck, J. T., Alexander, L. V., Durre, I. and Karoly, D. J. (2016). Extraordinary heat during the 1930s us dust bowl and associated large-scale conditions, *Climate Dynamics* **46**: 413–426.
**URL:** *https://link.springer.com/article/10.1007/s00382-015-2590-5*

Dong, Z., Wang, L., Sun, Y., Hu, T., Limsakul, A., Singhruck, P. and Pimonsree, S. (2021). Heatwaves in southeast asia and their changes in a warmer world, *Earth's Future* **9**.

Dosio, A., Mentaschi, L., Fischer, E. M. and Wyser, K. (2018). Extreme heat waves under 1.5 °c and 2 °c global warming, *Environmental Research Letters* **13**.

Drijfhout, S., van Oldenborgh, G. J. and Cimatoribus, A. (2012). Is a decline of amoc causing the warming hole above the north atlantic in observed and modeled warming patterns?, *Journal of Climate* **25**.

Dunn, R. J., Willett, K. M., Ciavarella, A. and Stott, P. A. (2017). Comparison of land surface humidity between observations and cmip5 models, *Earth System Dynamics* **8**.

Dunne, J. P., Hewitt, H. T., Arblaster, J., Bonou, F., Boucher, O., Cavazos, T., Durack, P. J., Hassler, B., Juckes, M., Miyakawa, T., Mizielinski, M., Naik, V., Nicholls, Z., O'Rourke, E., Pincus, R., Sanderson, B. M., Simpson, I. R. and Taylor, K. E. (2024). An evolving coupled model intercomparison project phase 7 (cmip7) and fast track in support of future climate assessment, *EGUsphere* pp. 1–51.
**URL:** *https://egusphere.copernicus.org/preprints/2024/egusphere-2024-3874/*

Ebi, K. L., Hasegawa, T., Hayes, K., Monaghan, A., Paz, S. and Berry, P. (2018). Health risks of warming of 1.5 °c, 2 °c, and higher, above pre-industrial temperatures.

Eischeid, J. K., Hoerling, M. P., Quan, X.-W., Kumar, A., Barsugli, J., Labe, Z., Kunkel, K., Schreck, C. J., Easterling, D., Zhang, T., Uehling, J. and Zhang, X. (2023). Why has the summertime central u.s. warming hole not disappeared?, *Journal of Climate* **36**: 7319–7336.
**URL:** *https://journals.ametsoc.org/view/journals/clim/aop/JCLI-D-22-0716.1/JCLI-D-22-0716.1.xml*

Eyring, V., Bony, S., Meehl, G. A., Senior, C. A., Stevens, B., Stouffer, R. J. and Taylor, K. E. (2016). Overview of the coupled model intercomparison project phase 6 (cmip6) experimental design and organization, *Geoscientific Model Development* **9**: 1937–1958.

Findell, K. L., Berg, A., Gentine, P., Krasting, J. P., Lintner, B. R., Malyshev, S., Santanello, J. A. and Shevliakova, E. (2017). The impact of anthropogenic land use and land cover change on regional climate extremes, *Nature Communications* **8**.

Fischer, E. M., Beyerle, U., Bloin-Wibe, L., Gessner, C., Humphrey, V., Lehner, F., Pendergrass, A. G., Sippel, S., Zeder, J. and Knutti, R. (2023). Storylines for unprecedented heatwaves based on ensemble boosting, *Nature Communications* **14**.

Fischer, E. M. and Knutti, R. (2015). Anthropogenic contribution to global occurrence of heavy-precipitation and high-temperature extremes, *Nature Climate Change* **5**.

Friedman, A. R., Hwang, Y. T., Chiang, J. C. and Frierson, D. M. (2013). Interhemispheric temperature asymmetry over the twentieth century and in future projections, *Journal of Climate* **26**.

Gaffen, D. J. and Ross, R. J. (1999). Climatology and trends of u.s. surface humidity and temperature, *Journal of Climate* **12**.

Garcia-Herrera, R., Díaz, J., Trigo, R. M., Luterbacher, J. and Fischer, E. M. (2010). A review of the european summer heat wave of 2003.

García-León, D., Casanueva, A., Standardi, G., Burgstall, A., Flouris, A. D. and Nybo, L. (2021). Current and projected regional economic impacts of heatwaves in europe, *Nature Communications* **12**.

Ghate, V. P., Carlton, A. G., Surleta, T. and Burns, A. M. (2022). Changes in aerosols, meteorology, and radiation in the southeastern u.s. warming hole region during 2000 to 2019, *Journal of Climate* **35**.

Gidden, M. J., Riahi, K., Smith, S. J., Fujimori, S., Luderer, G., Kriegler, E., Vuuren, D. P. V., Berg, M. V. D., Feng, L., Klein, D., Calvin, K., Doelman, J. C., Frank, S., Fricko, O., Harmsen, M., Hasegawa, T., Havlik, P., Hilaire, J., Hoesly, R., Horing, J., Popp, A., Stehfest, E. and Takahashi, K. (2019). Global emissions pathways under different socioeconomic scenarios for use in cmip6: A dataset of harmonized emissions trajectories through the end of the century, *Geoscientific Model Development* **12**.

Grose, M. R., Risbey, J. S. and Whetton, P. H. (2017). Tracking regional temperature projections from the early 1990s in light of variations in regional warming, including 'warming holes', *Climatic Change* **140**.

Habeeb, D., Vargo, J. and Stone, B. (2015). Rising heat wave trends in large us cities, *Natural Hazards* **76**.

Hamilton, E., Eade, R., Graham, R. J., Scaife, A. A., Smith, D. M., Maidens, A. and MacLachlan, C. (2012). Forecasting the number of extreme daily events on seasonal timescales, *Journal of Geophysical Research Atmospheres* **117**.

Harris, C. R., Millman, K. J., van der Walt, S. J., Gommers, R., Virtanen, P., Cournapeau, D., Wieser, E., Taylor, J., Berg, S., Smith, N. J., Kern, R., Picus, M., Hoyer, S., van Kerkwijk, M. H., Brett, M., Haldane, A., del Río, J. F., Wiebe, M., Peterson, P., Gérard-Marchant, P., Sheppard, K., Reddy, T., Weckesser, W., Abbasi, H., Gohlke, C. and Oliphant, T. E. (2020). Array programming with numpy, *Nature* **585**: 357.
**URL:** *https://doi.org/10.1038/s41586-020-2649-2*

Hausfather, Z. (2025). An assessment of current policy scenarios over the 21st century and the reduced plausibility of high-emissions pathways, *Dialogues on Climate Change* .

**URL:** *https://journals.sagepub.com/doi/full/10.1177/29768659241304854*

He, C., Chen, X., Collins, M., Song, F., Hu, Y., Jiang, X., Liu, Y., Ding, Y. and Zhou, W. (2024). Rising geopotential height under global warming, *Climate Dynamics* .

He, C., Clement, A. C., Cane, M. A., Murphy, L. N., Klavans, J. M. and Fenske, T. M. (2022). A north atlantic warming hole without ocean circulation, *Geophysical Research Letters* **49**.

Held, I. M., Guo, H., Adcroft, A., Dunne, J. P., Horowitz, L. W., Krasting, J., Shevliakova, E., Winton, M., Zhao, M., Bushuk, M., Wittenberg, A. T., Wyman, B., Xiang, B., Zhang, R., Anderson, W., Balaji, V., Donner, L., Dunne, K., Durachta, J., Gauthier, P. P., Ginoux, P., Golaz, J. C., Griffies, S. M., Hallberg, R., Harris, L., Harrison, M., Hurlin, W., John, J., Lin, P., Lin, S. J., Malyshev, S., Menzel, R., Milly, P. C., Ming, Y., Naik, V., Paynter, D., Paulot, F., Rammaswamy, V., Reichl, B., Robinson, T., Rosati, A., Seman, C., Silvers, L. G., Underwood, S. and Zadeh, N. (2019). Structure and performance of gfdl's cm4.0 climate model, *Journal of Advances in Modeling Earth Systems* **11**: 3691–3727.
**URL:** *https://agupubs.onlinelibrary.wiley.com/doi/10.1029/2019MS001829*

Henderson, S. B., McLean, K. E., Lee, M. J. and Kosatsky, T. (2022). Analysis of community deaths during the catastrophic 2021 heat dome, *Environmental Epidemiology* **6**.

Holmes, C. R., Woollings, T., Hawkins, E. and de Vries, H. (2016). Robust future changes in temperature variability under greenhouse gas forcing and the relationship with thermal advection, *Journal of Climate* **29**.

Horton, R. M., Mankin, J. S., Lesk, C., Coffel, E. and Raymond, C. (2016). A review of recent advances in research on extreme heat events.

Huang, J. and Dool, H. M. V. D. (1993). Monthly precipitation-temperature relations and temperature prediction over the united states, *Journal of Climate* **6**.

Hunter, J. D. (2007). Matplotlib: A 2d graphics environment, *Computing in Science and Engineering* **9**: 99–104.

Huntingford, C. and Lowe, J. (2007). "overshoot" scenarios and climate change, *Science* **316**.

Hurtt, G. C., Chini, L., Sahajpal, R., Frolking, S., Bodirsky, B. L., Calvin, K., Doelman, J. C., Fisk, J., Fujimori, S., Goldewijk, K. K., Hasegawa, T., Havlik, P., Heinimann, A., Humpenöder, F., Jungclaus, J., Kaplan, J. O., Kennedy, J., Krisztin, T., Lawrence, D., Lawrence, P., Ma, L., Mertz, O., Pongratz, J., Popp, A., Poulter, B., Riahi, K., Shevliakova, E., Stehfest, E., Thornton, P., Tubiello, F. N., van Vuuren, D. P. and Zhang, X. (2020). Harmonization of global land use change and management for the period 850-2100 (luh2) for cmip6, *Geoscientific Model Development* **13**.

IPCC (2021). Climate change 2021: The physical science basis. contribution of working group i to the sixth assessment report of the intergovernmental panel on climate change, *Technical report*.
**URL:** *https://doi.org/10.1017/9781009157896*

IPCC (2023a). *The Earth's Energy Budget, Climate Feedbacks and Climate Sensitivity.*
**URL:** *https://doi.org/10.1017/9781009157896.009*

IPCC (2023b). *Framing, Context, and Methods.*
**URL:** *https://doi.org/10.1017/9781009157896.003*

IPCC (2023c). *Future Global Climate: Scenario-based Projections and Near-term Information.*
**URL:** *https://doi.org/10.1017/9781009157896.006*

IPCC (2023d). *Weather and Climate Extreme Events in a Changing Climate.*
**URL:** *https://doi.org/10.1017/9781009157896.013*

Jain, S., Scaife, A. A., Shepherd, T. G., Deser, C., Dunstone, N., Schmidt, G. A., Trenberth, K. E. and Turkington, T. (2023). Importance of internal variability for climate model assessment, *npj Climate and Atmospheric Science* **6**.

James, R., Washington, R., Schleussner, C. F., Rogelj, J. and Conway, D. (2017). Characterizing half-a-degree difference: a review of methods for identifying regional climate responses to global warming targets.

Jia, L., Delworth, T. L., Kapnick, S., Yang, X., Johnson, N. C., Cooke, W., Lu, F., Harrison, M., Rosati,

A., Zeng, F., Mchugh, C., Wittenberg, A. T., Zhang, L., Murakami, H. and Tseng, K. C. (2022). Skillful seasonal prediction of north american summertime heat extremes, *Journal of Climate* **35**: 4331–4345.
**URL:** *https://journals.ametsoc.org/view/journals/clim/35/13/JCLI-D-21-0364.1.xml*

Jia, L., Delworth, T. L., Yang, X., Cooke, W., Johnson, N. C., McHugh, C. and Lu, F. (2023). Seasonal prediction of north american wintertime cold extremes in the gfdl spear forecast system, *Climate Dynamics* **61**.

Jia, L., Delworth, T. L., Yang, X., Cooke, W., Johnson, N. C., Zhang, L., Joh, Y., Lu, F. and McHugh, C. (2024). Seasonal predictions of summer compound humid heat extremes in the southeastern united states driven by sea surface temperatures, *npj Climate and Atmospheric Science 2024 7:1* **7**: 1–9.
**URL:** *https://www.nature.com/articles/s41612-024-00723-0*

Johnson, N. C., Wittenberg, A. T., Rosati, A. J., Delworth, T. L. and Cooke, W. (2022). Future changes in boreal winter enso teleconnections in a large ensemble of high-resolution climate simulations, *Frontiers in Climate* **4**.

Jones, C. G., Adloff, F., Booth, B. B. B., Cox, P. M., Eyring, V., Friedlingstein, P., Frieler, K., Hewitt, H. T., Jeffery, H. A., Joussaume, S., Koenigk, T., Lawrence, B. N., O'Rourke, E., Roberts, M. J., Sanderson, B. M., Séférian, R., Somot, S., Vidale, P. L., van Vuuren, D., Acosta, M., Bentsen, M., Bernardello, R., Betts, R., Blockley, E., Boé, J., Bracegirdle, T., Braconnot, P., Brovkin, V., Buontempo, C., Doblas-Reyes, F., Donat, M., Epicoco, I., Falloon, P., Fiore, S., Frölicher, T., Fučkar, N. S., Gidden, M. J., Goessling, H. F., Graversen, R. G., Gualdi, S., Gutiérrez, J. M., Ilyina, T., Jacob, D., Jones, C. D., Juckes, M., Kendon, E., Kjellström, E., Knutti, R., Lowe, J., Mizielinski, M., Nassisi, P., Obersteiner, M., Regnier, P., Roehrig, R., y Mélia, D. S., Schleussner, C.-F., Schulz, M., Scoccimarro, E., Terray, L., Thiemann, H., Wood, R. A., Yang, S. and Zaehle, S. (2024). Bringing it all together: science priorities for improved understanding of earth system change and to support international climate policy, *Earth System Dynamics* **15**: 1319–1351.
**URL:** *https://esd.copernicus.org/articles/15/1319/2024/*

Joshi, M. and Gregory, J. (2008). Dependence of the land-sea contrast in surface climate response on the nature of the forcing, *Geophysical Research Letters* **35**.

Joshi, M. M., Gregory, J. M., Webb, M. J., Sexton, D. M. and Johns, T. C. (2008). Mechanisms for the land/sea warming contrast exhibited by simulations of climate change, *Climate Dynamics* **30**.

Keellings, D. and Moradkhani, H. (2020). Spatiotemporal evolution of heat wave severity and coverage across the united states, *Geophysical Research Letters* **47**.

Keil, P., Mauritsen, T., Jungclaus, J., Hedemann, C., Olonscheck, D. and Ghosh, R. (2020). Multiple drivers of the north atlantic warming hole, *Nature Climate Change* **10**.

Kharin, V. V., Flato, G. M., Zhang, X., Gillett, N. P., Zwiers, F. and Anderson, K. J. (2018). Risks from climate extremes change differently from 1.5°c to 2.0°c depending on rarity, *Earth's Future* **6**.

Kim, S. K., Shin, J., An, S. I., Kim, H. J., Im, N., Xie, S. P., Kug, J. S. and Yeh, S. W. (2022). Widespread irreversible changes in surface temperature and precipitation in response to co2 forcing, *Nature Climate Change* **12**.

King, A. D., Donat, M. G., Lewis, S. C., Henley, B. J., Mitchell, D. M., Stott, P. A., Fischer, E. M. and Karoly, D. J. (2018). Reduced heat exposure by limiting global warming to 1.5 °c.

King, A. D. and Harrington, L. J. (2018). The inequality of climate change from 1.5 to 2°c of global warming.

Kirtman, B. P., Min, D., Infanti, J. M., Kinter, I. I. I. J. L., Paolino, D. A., Zhang, Q., van den Dool, H., Saha, S., Mendez, M. P., Becker, E., Peng, P., Tripp, P., Huang, J., DeWitt, D. G., Tippett, M. K., Barnston, A. G., Li, S., Rosati, A., Schubert, S. D., Rienecker, M., Suarez, M., Li, Z. E., Marshak, J., Lim, Y.-K., Tribbia, J., Pegion, K., Merryfield, W. J., Denis, B. and Wood, E. F.

(2014). The north american multimodel ensemble: Phase-1 seasonal-to-interannual prediction; phase-2 toward developing intraseasonal prediction.
**URL:** *http://journals.ametsoc.org/doi/abs/10.1175/BAMS-D-12-00050.1*

Koster, R. D., Dirmeyer, P. A., Guo, Z., Bonan, G., Chan, E., Cox, P., Gordon, C. T., Kanae, S., Kowalczyk, E., Lawrence, D., Liu, P., Lu, C. H., Malyshev, S., McAvaney, B., Mitchell, K., Mocko, D., Oki, T., Oleson, K., Pitman, A., Sud, Y. C., Taylor, C. M., Verseghy, D., Vasic, R., Xue, Y. and Yamada, T. (2004). Regions of strong coupling between soil moisture and precipitation, *Science* **305**.

Koster, R. D., Suarez, M. J., Higgins, R. W. and den Dool, H. M. V. (2003). Observational evidence that soil moisture variations affect precipitation, *Geophysical Research Letters* **30**.

Kriegler, E., Bauer, N., Popp, A., Humpenöder, F., Leimbach, M., Strefler, J., Baumstark, L., Bodirsky, B. L., Hilaire, J., Klein, D., Mouratiadou, I., Weindl, I., Bertram, C., Dietrich, J. P., Luderer, G., Pehl, M., Pietzcker, R., Piontek, F., Lotze-Campen, H., Biewald, A., Bonsch, M., Giannousakis, A., Kreidenweis, U., Müller, C., Rolinski, S., Schultes, A., Schwanitz, J., Stevanovic, M., Calvin, K., Emmerling, J., Fujimori, S. and Edenhofer, O. (2017). Fossil-fueled development (ssp5): An energy and resource intensive scenario for the 21st century, *Global Environmental Change* **42**: 297–315.

Kunkel, K. E., Liang, X. Z. and Zhu, J. (2010). Regional climate model projections and uncertainties of u.s. summer heat waves, *Journal of Climate* **23**.

Kunkel, K. E., Liang, X. Z., Zhu, J. and Lin, Y. (2006). Can cgcms simulate the twentieth-century "warning hole" in the central united states?, *Journal of Climate* **19**.

Labe, Z. M., Delworth, T. L., Johnson, N. C. and Cooke, W. F. (2024). Exploring a data-driven approach to identify regions of change associated with future climate scenarios, *Journal of Geophysical Research: Machine Learning and Computation* **1**: e2024JH000327.
**URL:** *https://agupubs.onlinelibrary.wiley.com/doi/10.1029/2024JH000327*

Labe, Z. M., Johnson, N. C. and Delworth, T. L. (2024). Changes in united states summer temperatures revealed by explainable neural networks, *Earth's Future* **12**: e2023EF003981.
**URL:** *https://onlinelibrary.wiley.com/doi/abs/10.1029/2023EF003981*

Lopez, H., West, R., Dong, S., Goni, G., Kirtman, B., Lee, S. K. and Atlas, R. (2018). Early emergence of anthropogenically forced heat waves in the western united states and great lakes, *Nature Climate Change* **8**.

Lu, F., Harrison, M. J., Rosati, A., Delworth, T. L., Yang, X., Cooke, W. F., Jia, L., McHugh, C., Johnson, N. C., Bushuk, M., Zhang, Y. and Adcroft, A. (2020). Gfdl's spear seasonal prediction system: Initialization and ocean tendency adjustment (ota) for coupled model predictions, *Journal of Advances in Modeling Earth Systems* **12**.
**URL:** *Lu2020spear*

Lyon, B. and Barnston, A. G. (2017). Diverse characteristics of u.s. summer heat waves, *Journal of Climate* **30**.

Lyon, B., Barnston, A. G., Coffel, E. and Horton, R. M. (2019). Projected increase in the spatial extent of contiguous us summer heat waves and associated attributes, *Environmental Research Letters* **14**.

Maher, N., Kay, J. E. and Capotondi, A. (2022). Modulation of enso teleconnections over north america by the pacific decadal oscillation, *Environmental Research Letters* **17**.

Manabe, S., Spelman, M. J. and Stouffer, R. J. (1992). Transient responses of a coupled ocean-atmosphere model to gradual changes of atmospheric co 2 . part ii: Seasonal response, *Journal of Climate* **5**.

Manabe, S. and Stouffer, R. J. (1980). Sensitivity of a global climate model to an increase of co2 concentration in the atmosphere., *Journal of Geophysical Research* .

Marcotullio, P. J., Keßler, C. and Fekete, B. M. (2021). The future urban heat-wave challenge in africa: Exploratory analysis, *Global Environmental Change* **66**.

Marvel, K., Su, W., Delgado, R., Aarons, S., Chatterjee, A., Garcia, M. E., Hausfather, Z., Hayhoe, K., Hence, D. A., Jewett, E. B., Robel, A., Singh, D., Tripati, A. and Vose, R. S. (2023). Chapter 2 : Climate trends. fifth national climate assessment, *Technical report*, U.S. Global Change Research Program.

Mascioli, N. R., Previdi, M., Fiore, A. M. and Ting, M. (2017). Timing and seasonality of the united states 'warming hole', *Environmental Research Letters* **12**.

McHugh, C. E., Delworth, T. L., Cooke, W. and Jia, L. (2023). Using large ensembles to examine historical and projected changes in record-breaking summertime temperatures over the contiguous united states, *Earth's Future* **11**: e2023EF003954.
**URL:** *https://onlinelibrary.wiley.com/doi/full/10.1029/2023EF003954*

McKinnon, K. A., Id, I. R. S. D. and Williams, A. P. (2024). The pace of change of summertime temperature extremes, *Proceedings of the National Academy of Sciences* **121**: e2406143121.
**URL:** *https://www.pnas.org/doi/abs/10.1073/pnas.2406143121*

Meehl, G. A., Arblaster, J. M. and Chung, C. T. (2015). Disappearance of the southeast u.s. "warming hole" with the late 1990s transition of the interdecadal pacific oscillation, *Geophysical Research Letters* **42**.

Meehl, G. A., Tebaldi, C. and Adams-Smith, D. (2016). Us daily temperature records past, present, and future, *Proceedings of the National Academy of Sciences of the United States of America* **113**.

Meehl, G. A., Tebaldi, C., Walton, G., Easterling, D. and McDaniel, L. (2009). Relative increase of record high maximum temperatures compared to record low minimum temperatures in the u.s., *Geophysical Research Letters* **36**.

Meinshausen, M., Nicholls, Z. R., Lewis, J., Gidden, M. J., Vogel, E., Freund, M., Beyerle, U., Gessner, C., Nauels, A., Bauer, N., Canadell, J. G., Daniel, J. S., John, A., Krummel, P. B., Luderer, G., Meinshausen, N., Montzka, S. A., Rayner, P. J., Reimann, S., Smith, S. J., Berg, M. V. D., Velders, G. J., Vollmer, M. K. and Wang, R. H. (2020). The shared socio-economic pathway (ssp) greenhouse gas concentrations and their extensions to 2500, *Geoscientific Model Development* **13**.

Meinshausen, M., Schleussner, C. F., Beyer, K., Bodeker, G., Boucher, O., Canadell, J. G., Daniel, J. S., Diongue-Niang, A., Driouech, F., Fischer, E., Forster, P., Grose, M., Hansen, G., Hausfather, Z., Ilyina, T., Kikstra, J. S., Kimutai, J., King, A. D., Lee, J. Y., Lennard, C., Lissner, T., Nauels, A., Peters, G. P., Pirani, A., Plattner, G. K., Pörtner, H., Rogelj, J., Rojas, M., Roy, J., Samset, B. H., Sanderson, B. M., Séférian, R., Seneviratne, S., Smith, C. J., Szopa, S., Thomas, A., Urge-Vorsatz, D., Velders, G. J., Yokohata, T., Ziehn, T. and Nicholls, Z. (2024). A perspective on the next generation of earth system model scenarios: Towards representative emission pathways (reps), *Geoscientific Model Development* **17**: 4533–4559.

Meinshausen, M., Vogel, E., Nauels, A., Lorbacher, K., Meinshausen, N., Etheridge, D. M., Fraser, P. J., Montzka, S. A., Rayner, P. J., Trudinger, C. M., Krummel, P. B., Beyerle, U., Canadell, J. G., Daniel, J. S., Enting, I. G., Law, R. M., Lunder, C. R., O'Doherty, S., Prinn, R. G., Reimann, S., Rubino, M., Velders, G. J., Vollmer, M. K., Wang, R. H. and Weiss, R. (2017). Historical greenhouse gas concentrations for climate modelling (cmip6), *Geoscientific Model Development* **10**.

Melnikova, I., Boucher, O., Cadule, P., Tanaka, K., Gasser, T., Hajima, T., Quilcaille, Y., Shiogama, H., Séférian, R., Tachiiri, K., Vuichard, N., Yokohata, T. and Ciais, P. (2022). Impact of bioenergy crop expansion on climate-carbon cycle feedbacks in overshoot scenarios, *Earth System Dynamics* **13**.

Menary, M. B., Robson, J., Allan, R. P., Booth, B. B., Cassou, C., Gastineau, G., Gregory, J., Hodson, D., Jones, C., Mignot, J., Ringer, M., Sutton, R., Wilcox, L. and Zhang, R. (2020). Aerosol-forced amoc changes in cmip6 historical simulations, *Geophysical Research Letters* **47**.

Meyer, A. L., Bentley, J., Odoulami, R. C., Pigot, A. L. and Trisos, C. H. (2022). Risks to biodiversity from temperature overshoot pathways, *Philosophical Transactions of the Royal Society B: Biological Sciences* **377**.

Milly, P. C., Malyshev, S. L., Shevliakova, E., Dunne, K. A., Findell, K. L., Gleeson, T., Liang, Z., Phillipps, P., Stouffer, R. J. and Swenson, S. (2014). An enhanced model of land water and energy for global hydrologic and earth-system studies, *Journal of Hydrometeorology* **15**.

Miralles, D. G., Gentine, P., Seneviratne, S. I. and Teuling, A. J. (2019). Land–atmospheric feedbacks during droughts and heatwaves: state of the science and current challenges, *Annals of the New York Academy of Sciences* **1436**.

Moreno-Chamarro, E., Marshall, J. and Delworth, T. L. (2020). Linking itcz migrations to the amoc and north atlantic/pacific sst decadal variability, *Journal of Climate* **33**.

Mueller, N. D., Butler, E. E., Mckinnon, K. A., Rhines, A., Tingley, M., Holbrook, N. M. and Huybers, P. (2016). Cooling of us midwest summer temperature extremes from cropland intensification, *Nature Climate Change* **6**.

Nature (2023). Reversing climate overshoot, *Nature Geoscience 2023 16:6* **16**: 467–467.
**URL:** *https://www.nature.com/articles/s41561-023-01213-3*

NCA4 (2018). Climate science special report: Fourth national climate assessment, volume i, *Technical report*, Global Change Research Program.
**URL:** *https://science2017.globalchange.gov*

O'Neill, B. C., Kriegler, E., Ebi, K. L., Kemp-Benedict, E., Riahi, K., Rothman, D. S., van Ruijven, B. J., van Vuuren, D. P., Birkmann, J., Kok, K., Levy, M. and Solecki, W. (2017). The roads ahead: Narratives for shared socioeconomic pathways describing world futures in the 21st century, *Global Environmental Change* **42**.

O'Neill, B. C., Kriegler, E., Riahi, K., Ebi, K. L., Hallegatte, S., Carter, T. R., Mathur, R. and van Vuuren, D. P. (2014). A new scenario framework for climate change research: The concept of shared socioeconomic pathways, *Climatic Change* **122**.

O'Neill, B. C., Tebaldi, C., Vuuren, D. P. V., Eyring, V., Friedlingstein, P., Hurtt, G., Knutti, R., Kriegler, E., Lamarque, J. F., Lowe, J., Meehl, G. A., Moss, R., Riahi, K. and Sanderson, B. M. (2016). The scenario model intercomparison project (scenariomip) for cmip6, *Geoscientific Model Development* **9**: 3461–3482.

Pan, Z. T., Arritt, R. W., Takle, E. S., Gutowski, W. J., Anderson, C. J. and Segal, M. (2004). Altered hydrologic feedback in a warming climate introduces a "warming hole", *Geophysical Research Letters* **31**: L17109.

Partridge, T. F., Winter, J. M., Osterberg, E. C., Hyndman, D. W., Kendall, A. D. and Magilligan, F. J. (2018a). Spatially distinct seasonal patterns and forcings of the u.s. warming hole, *Geophysical Research Letters* **45**: 2055–2063.
**URL:** *https://agupubs.onlinelibrary.wiley.com/doi/10.1002/2017GL076463*

Partridge, T. F., Winter, J. M., Osterberg, E. C., Hyndman, D. W., Kendall, A. D. and Magilligan, F. J. (2018b). Spatially distinct seasonal patterns and forcings of the u.s. warming hole, *Geophysical Research Letters* **45**.

Pedregosa, F., Varoquaux, G., Gramfort, A., Michel, V., Thirion, B., Grisel, O., Blondel, M., Prettenhofer, P., Weiss, R., Dubourg, V., Vanderplas, J., Passos, A., Cournapeau, D., Brucher, M., Perrot, M. and Édouard Duchesnay (2011). Scikit-learn: Machine learning in python, *Journal of Machine Learning Research* **12**.

Pepler, A. S., Díaz, L. B., Prodhomme, C., Doblas-Reyes, F. J. and Kumar, A. (2015). The ability of a multi-model seasonal forecasting ensemble to forecast the frequency of warm, cold and wet extremes, *Weather and Climate Extremes* **9**: 68–77.

Perkins-Kirkpatrick, S. E., Fischer, E. M., Angélil, O. and Gibson, P. B. (2017). The influence of internal climate variability on heatwave frequency trends, *Environmental Research Letters* **12**.

Perkins-Kirkpatrick, S. E. and Gibson, P. B. (2017). Changes in regional heatwave characteristics as a function of increasing global temperature, *Scientific Reports* **7**.

Perkins-Kirkpatrick, S. E. and Lewis, S. C. (2020). Increasing trends in regional heatwaves, *Nature Communications* **11**.

Peters, G. P. and Hausfather, Z. (2020). Emissions - the 'business as usual' story is misleading, *Nature*

**577**.

Peterson, T. C., Heim, R. R., Hirsch, R., Kaiser, D. P., Brooks, H., Diffenbaugh, N. S., Dole, R. M., Giovannettone, J. P., Guirguis, K., Karl, T. R., Katz, R. W., Kunkel, K., Lettenmaier, D., McCabe, G. J., Paciorek, C. J., Ryberg, K. R., Schubert, S., Silva, V. B., Stewart, B. C., Vecchia, A. V., Villarini, G., Vose, R. S., Walsh, J., Wehner, M., Wolock, D., Wolter, K., Woodhouse, C. A. and Wuebbles, D. (2013). Monitoring and understanding changes in heat waves, cold waves, floods, and droughts in the united states: State of knowledge, *Bulletin of the American Meteorological Society* **94**.

Pfleiderer, P., Schleussner, C.-F. and Sillmann, J. (2024). Limited reversal of regional climate signals in overshoot scenarios, *Environmental Research: Climate* **3**: 015005.

Phillips, A. S., Deser, C., Fasullo, J., Schneider, D. P. and Simpson, I. R. (2020). Assessing climate variability and change in model large ensembles: A user's guide to the climate variability diagnostics package for large ensembles version 1.0, *Technical report*, NCAR.
**URL:** *https://opensky.ucar.edu/islandora/object/manuscripts:1001*

Pielke, R., Burgess, M. G. and Ritchie, J. (2022). Plausible 2005–2050 emissions scenarios project between 2c and 3c of warming by 2100, *Environmental Research Letters* **17**: 024027.
**URL:** *https://iopscience.iop.org/article/10.1088/1748-9326/ac4ebf/meta*

Pierce, D. W., Westerling, A. L. and Oyler, J. (2013). Future humidity trends over the western united states in the cmip5 global climate models and variable infiltration capacity hydrological modeling system, *Hydrology and Earth System Sciences* **17**.

Portmann, R. W., Solomon, S. and Hegerl, G. C. (2009). Spatial and seasonal patterns in climate change, temperatures, and precipitation across the united states, *Proceedings of the National Academy of Sciences of the United States of America* **106**: 7324–7329.

Rastogi, D., Lehner, F. and Ashfaq, M. (2020). Revisiting recent u.s. heat waves in a warmer and more humid climate, *Geophysical Research Letters* **47**.

Raymond, C., Matthews, T. and Horton, R. M. (2020). The emergence of heat and humidity too severe for human tolerance, *Science Advances* **6**.

Rennie, J., Bell, J. E., Kunkel, K. E., Herring, S., Cullen, H. and Abadi, A. M. (2019). Development of a submonthly temperature product to monitor near-real-time climate conditions and assess long-term heat events in the united states, *Journal of Applied Meteorology and Climatology* **58**.

Riahi, K., van Vuuren, D. P., Kriegler, E., Edmonds, J., O'Neill, B. C., Fujimori, S., Bauer, N., Calvin, K., Dellink, R., Fricko, O., Lutz, W., Popp, A., Cuaresma, J. C., KC, S., Leimbach, M., Jiang, L., Kram, T., Rao, S., Emmerling, J., Ebi, K., Hasegawa, T., Havlik, P., Humpenöder, F., Silva, L. A. D., Smith, S., Stehfest, E., Bosetti, V., Eom, J., Gernaat, D., Masui, T., Rogelj, J., Strefler, J., Drouet, L., Krey, V., Luderer, G., Harmsen, M., Takahashi, K., Baumstark, L., Doelman, J. C., Kainuma, M., Klimont, Z., Marangoni, G., Lotze-Campen, H., Obersteiner, M., Tabeau, A. and Tavoni, M. (2017). The shared socioeconomic pathways and their energy, land use, and greenhouse gas emissions implications: An overview, *Global Environmental Change* **42**: 153–168.

Risbey, J. S., Irving, D. B., Squire, D. T., Matear, R. J., Monselesan, D. P., Pook, M. J., Ramesh, N., Richardson, D. and Tozer, C. R. (2023). A large ensemble illustration of how record-shattering heat records can endure, *Environmental Research: Climate* **2**.

Roberts, M. J., Jackson, L. C., Roberts, C. D., Meccia, V., Docquier, D., Koenigk, T., Ortega, P., Moreno-Chamarro, E., Bellucci, A., Coward, A., Drijfhout, S., Exarchou, E., Gutjahr, O., Hewitt, H., Iovino, D., Lohmann, K., Putrasahan, D., Schiemann, R., Seddon, J., Terray, L., Xu, X., Zhang, Q., Chang, P., Yeager, S. G., Castruccio, F. S., Zhang, S. and Wu, L. (2020). Sensitivity of the atlantic meridional overturning circulation to model resolution in cmip6 highresmip simulations and implications for future changes, *Journal of Advances in Modeling Earth Systems* **12**.

Rogers, C. D., Ting, M., Li, C., Kornhuber, K., Coffel, E. D., Horton, R. M., Raymond, C. and Singh, D. (2021). Recent increases in exposure to extreme humid-heat events disproportionately affect populated regions, *Geophysical Research Letters* **48**.

Rogers, J. C. (2013). The 20th century cooling trend over the southeastern united states, *Climate Dynamics* **40**.

Roldán-Gómez, P. J., Luca, P. D., Bernardello, R. and Donat, M. G. (2024). Regional non-reversibility of mean and extreme climate conditions in cmip6 overshoot scenarios linked to large-scale temperature asymmetries, *Earth System Dynamics Discussions* .
**URL:** *https://doi.org/10.5194/esd-2024-26*

Rossum, G. V. and Drake, F. L. (2009). *Python 3 Reference Manual [Software]*, CreateSpace.

Santana-Falcón, Y., Yamamoto, A., Lenton, A., Jones, C. D., Burger, F. A., John, J. G., Tjiputra, J., Schwinger, J., Kawamiya, M., Frölicher, T. L., Ziehn, T. and Séférian, R. (2023). Irreversible loss in marine ecosystem habitability after a temperature overshoot, *Communications Earth and Environment* **4**.

Savitzky, A. and Golay, M. J. (1964). Smoothing and differentiation of data by simplified least squares procedures, *Analytical Chemistry* **36**.

Schleussner, C.-F., Ganti, G., Lejeune, Q., Zhu, B., Pfleiderer, P., Prütz, R., Ciais, P., Frölicher, T. L., Fuss, S., Gasser, T., Gidden, M. J., Kropf, C. M., Lacroix, F., Lamboll, R., Martyr, R., Maussion, F., McCaughey, J. W., Meinshausen, M., Mengel, M., Nicholls, Z., Quilcaille, Y., Sanderson, B., Seneviratne, S. I., Sillmann, J., Smith, C. J., Steinert, N. J., Theokritoff, E., Warren, R., Price, J. and Rogelj, J. (2024). Overconfidence in climate overshoot, *Nature* **634**: 366–373.
**URL:** *https://www.nature.com/articles/s41586-024-08020-9*

Schleussner, C. F., Lissner, T. K., Fischer, E. M., Wohland, J., Perrette, M., Golly, A., Rogelj, J., Childers, K., Schewe, J., Frieler, K., Mengel, M., Hare, W. and Schaeffer, M. (2016). Differential climate impacts for policy-relevant limits to global warming: The case of 1.5 °c and 2 °c, *Earth System Dynamics* **7**: 327–351.

Schreck, C. J., Easterling, D. R., Barsugli, J., Coates, D. A., Hoell, A., Johnson, N. C., Kunkel, K. E., Labe, Z. M., Uehling, J., Vose, R. S. and Zhang, X. (2024). A rapid response process for evaluating causes of extreme temperature events in the united states: the 2023 texas/louisiana heat wave as a prototype, *Environmental Research: Climate* **3**: 1–16.
**URL:** *https://iopscience.iop.org/article/10.1088/2752-5295/ad8028*

Schulzweida, U. (2019). Cdo user guide [software], *Zenodo* .
**URL:** *https://zenodo.org/record/2558193*

Seneviratne, S. I., Donat, M. G., Pitman, A. J., Knutti, R. and Wilby, R. L. (2016). Allowable co2 emissions based on regional and impact-related climate targets.

Seneviratne, S. I. and Hauser, M. (2020). Regional climate sensitivity of climate extremes in cmip6 versus cmip5 multimodel ensembles, *Earth's Future* **8**.

Shiva, J. S., Chandler, D. G. and Kunkel, K. E. (2019). Localized changes in heat wave properties across the united states, *Earth's Future* **7**.

Smith, T. T., Zaitchik, B. F. and Gohlke, J. M. (2013). Heat waves in the united states: Definitions, patterns and trends, *Climatic Change* **118**.

Suarez-Gutierrez, L., Li, C., Müller, W. A. and Marotzke, J. (2018). Internal variability in european summer temperatures at 1.5 °c and 2 °c of global warming, *Environmental Research Letters* **13**.

Suarez-Gutierrez, L., Müller, W. A., Li, C. and Marotzke, J. (2020). Hotspots of extreme heat under global warming, *Climate Dynamics* **55**.

Sutton, R. T., Dong, B. and Gregory, J. M. (2007). Land/sea warming ratio in response to climate change: Ipcc ar4 model results and comparison with observations, *Geophysical Research Letters* **34**.

Tebaldi, C., Debeire, K., Eyring, V., Fischer, E., Fyfe, J., Friedlingstein, P., Knutti, R., Lowe, J., O'Neill, B., Sanderson, B., Vuuren, D. V., Riahi, K., Meinshausen, M., Nicholls, Z., Tokarska, K., Hurtt, G., Kriegler, E., Meehl, G., Moss, R., Bauer, S., Boucher, O., Brovkin, V., Yhb, Y., Dix, M., Gualdi, S., Guo, H., John, J., Kharin, S., Kim, Y. H., Koshiro, T., Ma, L., Olivié, D., Panickal, S., Qiao, F., Rong, X., Rosenbloom, N., Schupfner, M., Séférian, R., Sellar, A., Semmler, T., Shi, X., Song, Z., Steger, C., Stouffer, R., Swart, N., Tachiiri, K., Tang, Q., Tatebe, H., Voldoire, A., Volodin, E., Wyser, K., Xin, X., Yang, S., Yu, Y. and Ziehn, T. (2021). Climate model projections from the scenario model intercomparison project (scenariomip) of cmip6, *Earth System Dynamics* **12**.

Tebaldi, C. and Friedlingstein, P. (2013). Delayed detection of climate mitigation benefits due to climate inertia and variability, *Proceedings of the National Academy of Sciences of the United States of America* **110**.

Tebaldi, C. and Wehner, M. F. (2018). Benefits of mitigation for future heat extremes under rcp4.5 compared to rcp8.5, *Climatic Change* **146**.

Thomas, N. P., Bosilovich, M. G., Collow, A. B. M., Koster, R. D., Schubert, S. D., Dezfuli, A. and Mahanama, S. P. (2020). Mechanisms associated with daytime and nighttime heat waves over the contiguous united states, *Journal of Applied Meteorology and Climatology* **59**.

Thompson, V., Mitchell, D., Hegerl, G. C., Collins, M., Leach, N. J. and Slingo, J. M. (2023). The most at-risk regions in the world for high-impact heatwaves, *Nature Communications* **14**.

Thyng, K., Greene, C., Hetland, R., Zimmerle, H. and DiMarco, S. (2016). True colors of oceanography: Guidelines for effective and accurate colormap selection, *Oceanography* **29**: 9–13.
**URL:** *https://tos.org/oceanography/article/true-colors-of-oceanography-guidelines-for-effective-and-accurate-colormap*

Tian, H., Pan, N., Thompson, R. L., Canadell, J. G., Suntharalingam, P., Regnier, P., Davidson, E. A., Prather, M., Ciais, P., Muntean, M., Pan, S., Winiwarter, W., Zaehle, S., Zhou, F., Jackson, R. B., Bange, H. W., Berthet, S., Bian, Z., Bianchi, D., Bouwman, A. F., Buitenhuis, E. T., Dutton, G., Hu, M., Ito, A., Jain, A. K., Jeltsch-Thömmes, A., Joos, F., Kou-Giesbrecht, S., Krummel, P. B., Lan, X., Landolfi, A., Lauerwald, R., Li, Y., Lu, C., Maavara, T., Manizza, M., Millet, D. B., Mühle, J., Patra, P. K., Peters, G. P., Qin, X., Raymond, P., Resplandy, L., Rosentreter, J. A., Shi, H., Sun, Q., Tonina, D., Tubiello, F. N., Werf, G. R. V. D., Vuichard, N., Wang, J., Wells, K. C., Western, L. M., Wilson, C., Yang, J., Yao, Y., You, Y. and Zhu, Q. (2024). Global nitrous oxide budget (1980-2020), *Earth System Science Data* **16**.

Tian, Y., Kleidon, A., Lesk, C., Zhou, S., Luo, X., Ghausi, S. A., Wang, G., Zhong, D. and Zscheischler, J. (2024). Characterizing heatwaves based on land surface energy budget, *Communications Earth and Environment* **5**: 1–9.
**URL:** *https://www.nature.com/articles/s43247-024-01784-y*

van der Velden, E. (2020). Cmasher: Scientific colormaps for making accessible, informative and 'cmashing' plots, *Journal of Open Source Software* **5**: 2004.
**URL:** *https://joss.theoj.org/papers/10.21105/joss.02004*

Vicente-Serrano, S. M., Nieto, R., Gimeno, L., Azorin-Molina, C., Drumond, A., Kenawy, A. E., Dominguez-Castro, F., Tomas-Burguera, M. and Peña-Gallardo, M. (2018). Recent changes of relative humidity: Regional connections with land and ocean processes, *Earth System Dynamics* **9**.

Virtanen, P., Gommers, R., Oliphant, T. E., Haberland, M., Reddy, T., Cournapeau, D., Burovski, E., Peterson, P., Weckesser, W., Bright, J., van der Walt, S. J., Brett, M., Wilson, J., Millman, K. J., Mayorov, N., Nelson, A. R., Jones, E., Kern, R., Larson, E., Carey, C. J., İlhan Polat, Feng, Y., Moore, E. W., VanderPlas, J., Laxalde, D., Perktold, J., Cimrman, R., Henriksen, I., Quintero, E. A., Harris, C. R., Archibald, A. M., Ribeiro, A. H., Pedregosa, F., van Mulbregt, P., Vijaykumar, A., Bardelli, A. P., Rothberg, A., Hilboll, A., Kloeckner, A., Scopatz, A., Lee, A., Rokem, A., Woods, C. N., Fulton, C., Masson, C., Häggström, C., Fitzgerald, C., Nicholson, D. A., Hagen, D. R., Pasechnik, D. V., Olivetti, E., Martin, E., Wieser, E., Silva, F., Lenders, F., Wilhelm, F., Young, G., Price, G. A., Ingold, G. L., Allen, G. E., Lee, G. R., Audren, H., Probst, I., Dietrich, J. P., Silterra, J., Webber, J. T., Slavič, J., Nothman, J., Buchner, J., Kulick, J., Schönberger, J. L., de Miranda Cardoso, J. V., Reimer, J., Harrington, J., Rodríguez, J. L. C., Nunez-Iglesias, J., Kuczynski, J., Tritz, K., Thoma, M., Newville, M., Kümmerer, M., Bolingbroke, M., Tartre, M., Pak, M., Smith, N. J., Nowaczyk, N., Shebanov, N., Pavlyk, O., Brodtkorb, P. A., Lee, P., McGibbon, R. T., Feldbauer, R., Lewis, S., Tygier, S., Sievert, S., Vigna, S., Peterson, S., More, S., Pudlik, T., Oshima, T., Pingel, T. J., Robitaille, T. P., Spura, T., Jones, T. R., Cera, T., Leslie, T., Zito, T., Krauss, T., Upadhyay, U., Halchenko, Y. O. and Vázquez-Baeza, Y. (2020). Scipy 1.0: fundamental algorithms for scientific computing in python, *Nature Methods* **17**.

Wallace, C. J. and Joshi, M. (2018). Comparison of land-ocean warming ratios in updated observed records and cmip5 climate models, *Environmental Research Letters* **13**.

Wanyama, D., Bunting, E. L., Weil, N. and Keellings, D. (2023). Delineating and characterizing changes in heat wave events across the united states climate regions, *Climatic Change* **176**.

Wartenburger, R., Hirschi, M., Donat, M. G., Greve, P., Pitman, A. J. and Seneviratne, S. I. (2017). Changes in regional climate extremes as a function of global mean temperature: An interactive plotting framework, *Geoscientific Model Development* **10**.

Wehner, M. F. (2020). Characterization of long period return values of extreme daily temperature and precipitation in the cmip6 models: Part 2, projections of future change, *Weather and Climate Extremes* **30**.

Weijer, W., Cheng, W., Garuba, O. A., Hu, A. and Nadiga, B. T. (2020). Cmip6 models predict significant 21st century decline of the atlantic meridional overturning circulation, *Geophysical Research Letters* **47**.

Wilks, D. S. (2006). On "field significance" and the false discovery rate, *Journal of Applied Meteorology and Climatology* **45**: 1181–1189.
**URL:** *http://journals.ametsoc.org/doi/abs/10.1175/JAM2404.1*

Wilks, D. S. (2016). "the stippling shows statistically significant grid points": How research results are routinely overstated and overinterpreted, and what to do about it, *Bulletin of the American Meteorological Society* **97**: 2263–2273.
**URL:** *http://journals.ametsoc.org/doi/10.1175/BAMS-D-15-00267.1*

Wobus, C., Zarakas, C., Malek, P., Sanderson, B., Crimmins, A., Kolian, M., Sarofim, M. and Weaver, C. P. (2018). Reframing future risks of extreme heat in the united states, *Earth's Future* **6**.

Wu, P., Ridley, J., Pardaens, A., Levine, R. and Lowe, J. (2015). The reversibility of co2 induced climate change, *Climate Dynamics* **45**.

Wu, P., Wood, R., Ridley, J. and Lowe, J. (2010). Temporary acceleration of the hydrological cycle in response to a co 2 rampdown, *Geophysical Research Letters* **37**.

Yang, X., Delworth, T. L., Zeng, F., Zhang, L., Cooke, W. F., Harrison, M. J., Rosati, A., Underwood, S., Compo, G. P. and McColl, C. (2021). On the development of gfdl's decadal prediction system: Initialization approaches and retrospective forecast assessment, *Journal of Advances in Modeling Earth Systems* **13**.

Yang, Z., Dominguez, F. and Zeng, X. (2019). Large and local-scale features associated with heat waves in the united states in reanalysis products and the narccap model ensemble, *Climate Dynamics* **52**.

Yoon, D., Chen, J. H. and Seo, E. (2024). Contribution of land-atmosphere coupling in 2022 conus compound drought-heatwave events and implications for forecasting, *Weather and Climate Extremes* **46**: 100722.

Yu, B., Li, G., Chen, S. and Lin, H. (2020). The role of internal variability in climate change projections of north american surface air temperature and temperature extremes in canesm2 large ensemble simulations, *Climate Dynamics* **55**: 869–885.
**URL:** *https://link.springer.com/article/10.1007/s00382-020-05296-1*

Zarakas, C. M., Swann, A. L., Laguë, M. M., Armour, K. C. and Randerson, J. T. (2020). Plant physiology increases the magnitude and spread of the transient climate response to co2 in cmip6 earth system models, *Journal of Climate* **33**.

Zender, C. S. (2008). Analysis of self-describing gridded geoscience data with netcdf operators (nco), *Environmental Modelling and Software* **23**.

Zhang, S., Hu, Y., Zhang, J. and Xia, Y. (2024). Attribution of biases of interhemispheric temperature contrast in cmip6 models, *Advances in Atmospheric Sciences* **41**.

Zhao, M., Golaz, J. C., Held, I. M., Guo, H., Balaji, V., Benson, R., Chen, J. H., Chen, X., Donner, L. J., Dunne, J. P., Dunne, K., Durachta, J., Fan, S. M., Freidenreich, S. M., Garner, S. T., Ginoux, P., Harris, L. M., Horowitz, L. W., Krasting, J. P., Langenhorst, A. R., Liang, Z., Lin, P., Lin, S. J., Malyshev, S. L., Mason, E., Milly, P. C., Ming, Y., Naik, V., Paulot, F., Paynter, D., Phillipps, P., Radhakrishnan, A., Ramaswamy, V., Robinson, T., Schwarzkopf, D., Seman, C. J., Shevliakova, E., Shen, Z., Shin, H., Silvers, L. G., Wilson, J. R., Winton, M., Wittenberg, A. T., Wyman, B. and Xiang, B. (2018a). The gfdl global atmosphere and land model am4.0/lm4.0: 1. simulation characteristics with prescribed ssts, *Journal of Advances in Modeling Earth Systems* **10**: 691–734.
**URL:** *https://agupubs.onlinelibrary.wiley.com/doi/10.1002/2017MS001208*

Zhao, M., Golaz, J. C., Held, I. M., Guo, H., Balaji, V., Benson, R., Chen, J. H., Chen, X., Donner, L. J., Dunne, J. P., Dunne, K., Durachta, J., Fan, S. M., Freidenreich, S. M., Garner, S. T., Ginoux, P., Harris, L. M., Horowitz, L. W., Krasting, J. P., Langenhorst, A. R., Liang, Z., Lin, P., Lin, S. J., Malyshev, S. L., Mason, E., Milly, P. C., Ming, Y., Naik, V., Paulot, F., Paynter, D., Phillipps, P., Radhakrishnan, A., Ramaswamy, V., Robinson, T., Schwarzkopf, D., Seman, C. J., Shevliakova, E., Shen, Z., Shin, H., Silvers, L. G., Wilson, J. R., Winton, M., Wittenberg, A. T., Wyman, B. and Xiang, B. (2018b). The gfdl global atmosphere and land model am4.0/lm4.0: 2. model description, sensitivity studies, and tuning strategies, *Journal of Advances in Modeling Earth Systems* **10**: 735–769.
**URL:** *https://agupubs.onlinelibrary.wiley.com/doi/10.1002/2017MS001209*

Zhuang, Y., Fu, R., Santer, B. D., Dickinson, R. E. and Hall, A. (2021). Quantifying contributions of natural variability and anthropogenic forcings on increased fire weather risk over the western united states, *Proceedings of the National Academy of Sciences of the United States of America* **118**.

# Supporting information for "Large reductions in United States heat extremes found in overshoot simulations with SPEAR"

**Zachary M. Labe[1,2,*], Thomas L. Delworth[1], Nathaniel C. Johnson[1], Bor-Ting Jong[2], Colleen E. McHugh[1], William F. Cooke[1], and Liwei Jia[1]**

[1] NOAA/OAR/Geophysical Fluid Dynamics Laboratory, Princeton, NJ, USA

[2] Atmospheric and Oceanic Sciences Program, Princeton University, Princeton, NJ, USA

*E-mail: `zacklabe.climate@gmail.com`

Submitted to: *Environ. Res. Climate*

**Contents of this file:**

## Section S1. Table S1:

**Table S1.** Summary of the different climate change scenarios evaluated in this study with the GFDL SPEAR model (Delworth et al., 2020). The table is adapted from Labe et al. (2024).

| GFDL SPEAR Large Ensemble | Radiative Forcing Scenario | Years | Ensemble Members |
|---|---|---|---|
| SPEAR_MED_HISTORICAL | Historial Forcing from CMIP6 | 1921-2014 | 30 |
| SPEAR_MED_SSP245 | SSP2-4.5 from CMIP6 | 2015-2100 | 30 |
| SPEAR_MED_SSP585 | SSP5-8.5 from CMIP6 | 2015-2100 | 30 |
| SPEAR_MED_SSP534OS | SSP5-3.4OS from CMIP6 | 2015-2100 | 30 |
| SPEAR_MED_SSP534OS_10ye | SSP5-3.4OS, but with $CO_2$/$CH_4$ mitigation starting 10 years earlier (_10ye) | 2031-2100 | 30 |

**Section S2. Figures S1-S12:**

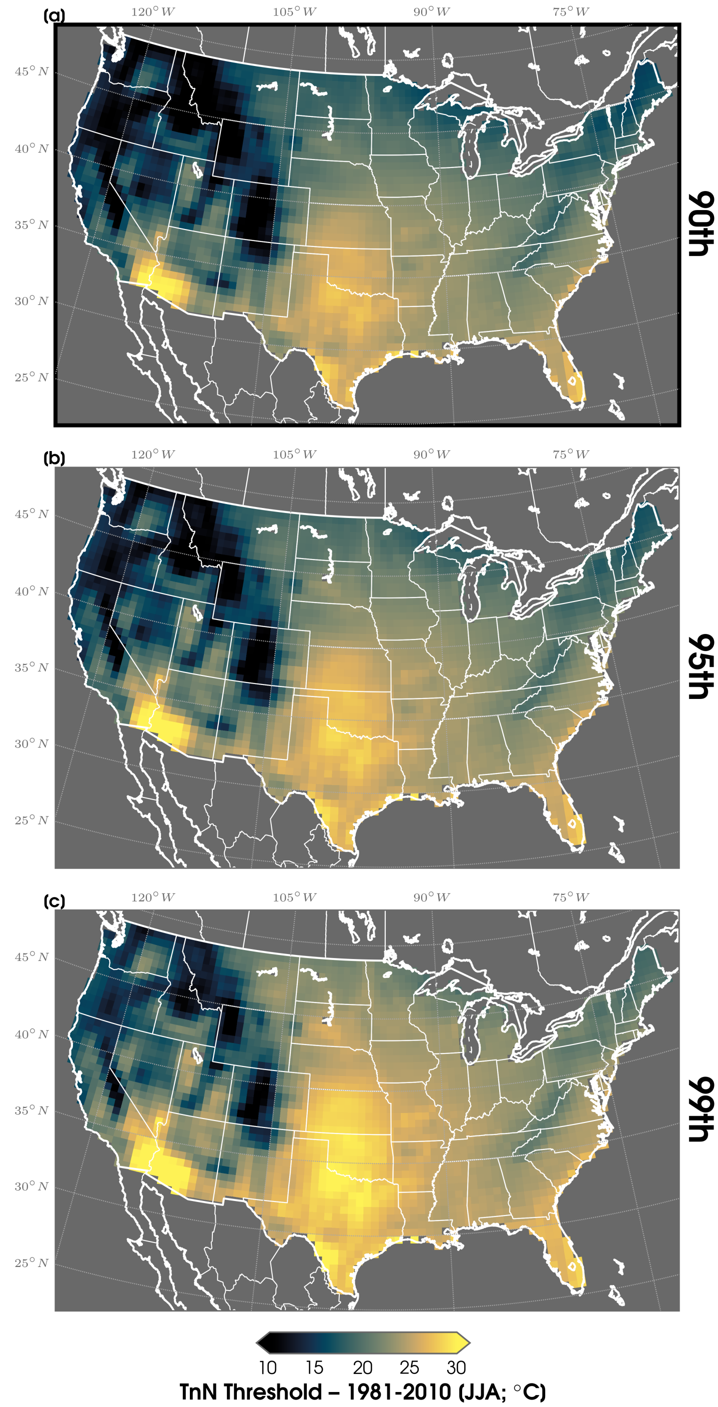


**Figure S1.** (a) CONUS map of the raw minimum daily temperature (nighttime) heat extreme thresholds in summer for the 90th percentile (Tn90), 95th percentile (Tn95), and 99th percentile (Tn99). This static threshold is calculated based on the distribution of daily maximum temperatures from June to August (JJA) and across all 30 ensemble members using the SPEAR historical run from 1981 to 2010. This threshold is computed separately at each grid point.

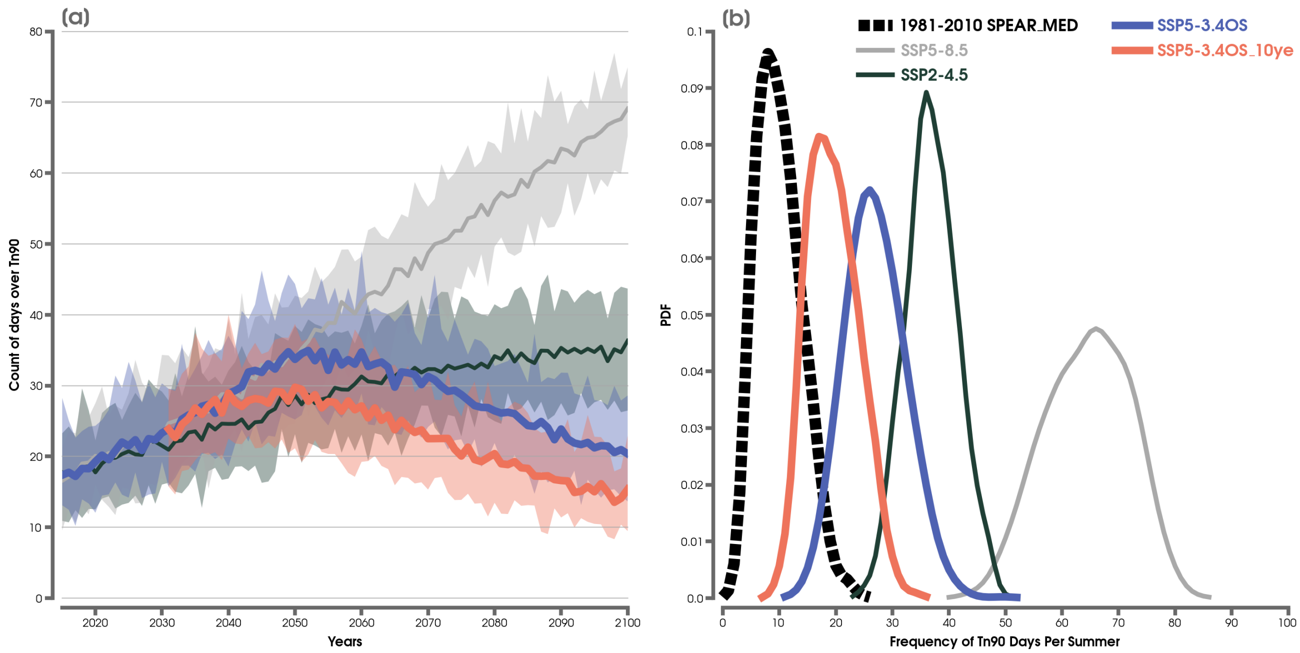


**Figure S2.** (a) Time series of the count of JJA nighttime heat extremes (Tn90) averaged for CONUS from 2015 to 2100 for the ensemble mean of SPEAR following the SSP5-8.5 climate scenario (light gray line), the SSP2-4.5 climate scenario (dark green line), the SSP5-3.4OS climate scenario (purple line) and from 2031 to 2100 for the SSP5-3.4OS_10ye climate scenario (orange line). The spread across ensemble members is shown with the lighter shading for each respective experiment. (b) Probability density functions (PDFs) of the distribution of the average frequency of mean CONUS Tn90 days in JJA over the years 1981 to 2010 using the historical scenario (dashed black curve), the SSP5-8.5 scenario from 2071 to 2100 (light gray surve), the SSP2-4.5 scenario from 2071 to 2100 (orange curve), the SSP5-3.4OS scenario from 2071 to 2100 (dark green curve), and the SSP5-3.4OS_10ye scenario from 2071 to 2100 (purple curve). The non-parametric PDFs are constructed using gaussian kernel density estimation with the optimal bandwidth determined through cross-validation. Each PDF considers data from all ensemble members in each 30-year period.

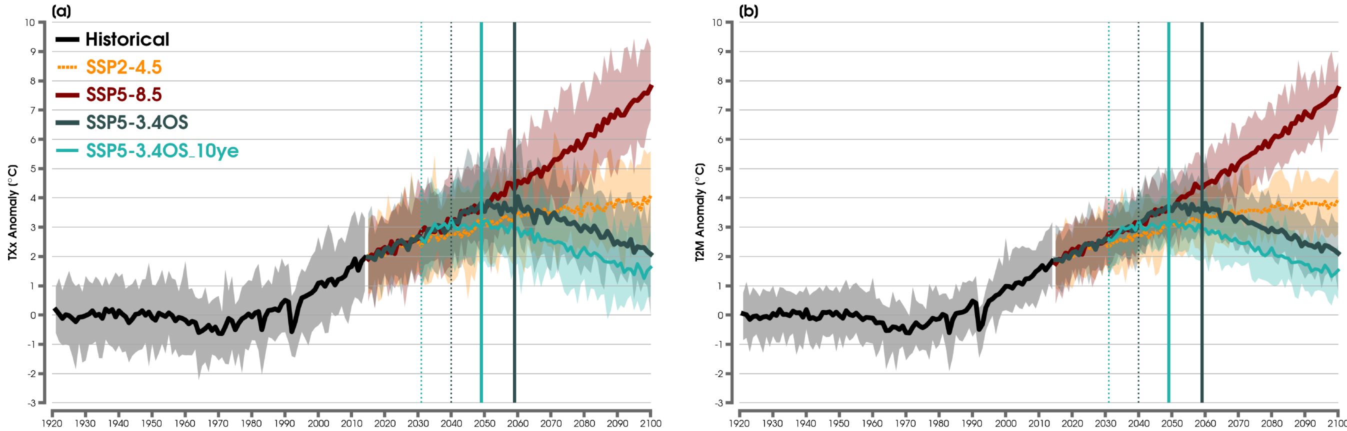


**Figure S3.** (a) Time series of the seasonally-averaged JJA highest daily maximum temperature (TXx) anomaly for the contiguous United States (CONUS) from 2015 to 2100 for the ensemble mean of SPEAR following the SSP5-8.5 climate scenario (solid red line), the SSP2-4.5 climate scenario (dashed orange line), the SSP5-3.4OS climate scenario (solid dark green line) and from 2031 to 2100 for the SSP5-3.4OS_10ye climate scenario (solid light green line). The spread across SPEAR ensemble members is shown with the lighter shading for each respective experiment. Anomalies are computed with respect to the 1921-1950 climatological time mean. The dashed vertical lines indicate the start of climate mitigation in 2031 (light green) and 2040 (dark green) for SSP5-3.4OS_10ye and SSP5-3.4OS, respectively. The solid vertical lines indicate the maximum (max) ensemble-mean global temperature for SSP5-3.4OS_10ye (light green) and SSP5-3.4OS (dark green), respectively. (b) Same as (a), but for the JJA mean temperature (T2M) anomaly.

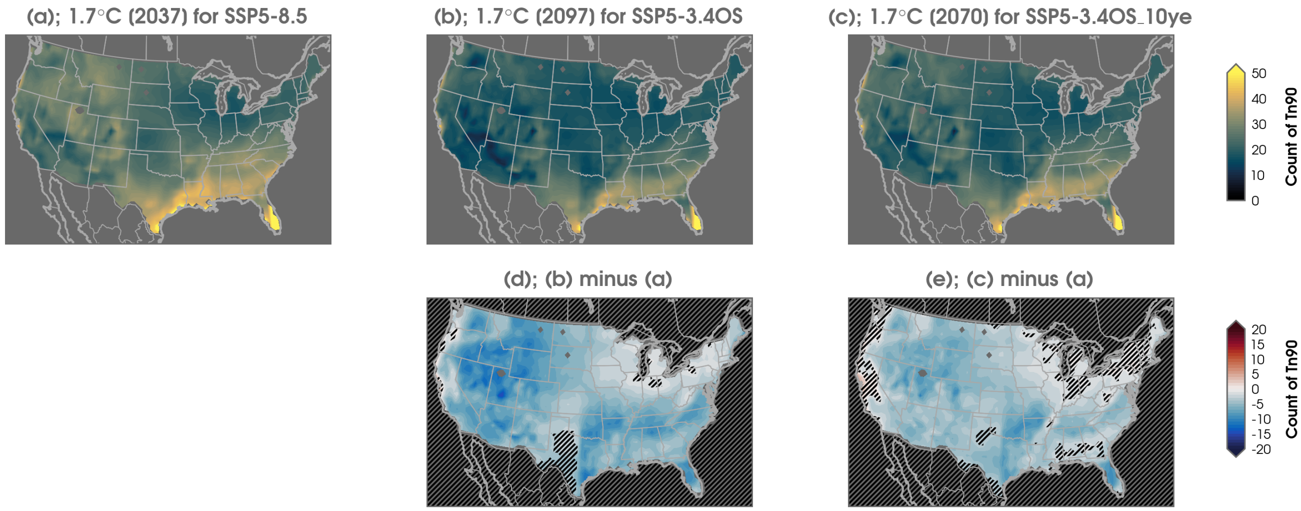


**Figure S4.** (a) Change in the number of Tn90 days at a GWL of 1.7°C for the SSP5-8.5 climate scenario. (b) Same as (a), but for the SSP5-3.4OS scenario after the influences of climate mitigation efforts are underway (see text for details). (c) Same as (b), but for the SSP5-3.4OS_10ye scenario. (d) Difference in panel (b) minus (a). (e) Difference in panel (c) minus (a). All anomalies are computed with respect to the 1921-1950 climatological time mean from the SPEAR historical scenario. Each composite map is calculated as the average of ±2 years around the ensemble mean year closest to an annual mean GMST of 1.7°C per climate scenario. Statistically significant differences in panels (d) and (e) are shown with the anomaly color shading. Non-significant regions are denoted with black hatching, which is assessed using a two-sided Student's $t$ test and after adjusting for field significance using a false discovery rate (FDR; Benjamini and Hochberg, 1995; Wilks, 2006; Wilks, 2016) (i.e., a FDR-adjusted $p$-value less than 0.05)

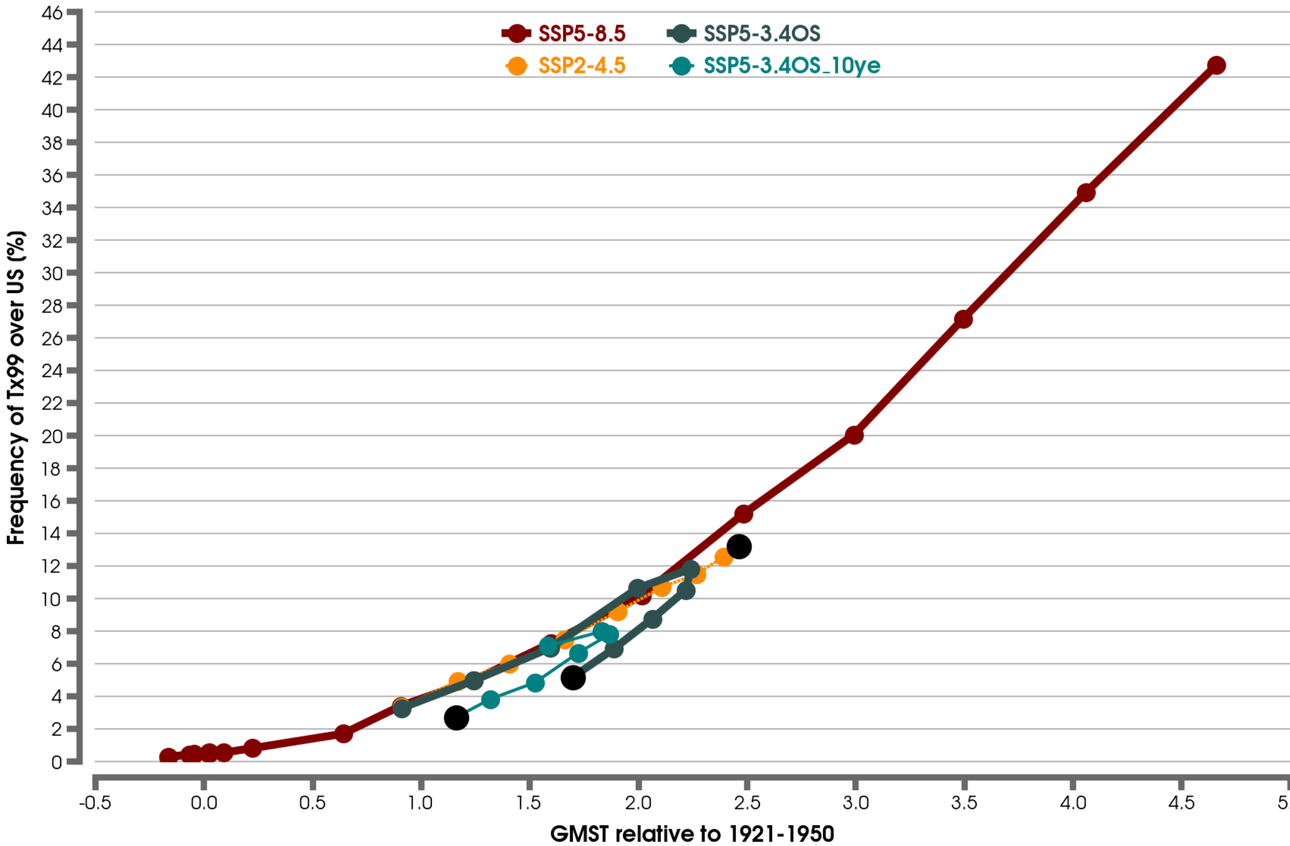


**Figure S5.** Decadal average of the frequency of JJA Tx99 heat extreme days averaged across the CONUS as a function of JJA mean GMST for the ensemble mean of the SPEAR future climate scenario of SSP5-8.5 (solid red line), SSP2-4.5 (dashed orange line), SSP5-3.4OS (solid dark green line), and SSP5-3.4OS_10ye (thin light green line). GMST anomalies are computed with respect to their 1921-1950 climatological time means. The historical climate scenario is used to calculate the decadal means starting in 1921 and then concatenated with each future scenario which begins in 2015. The black scatter points indicate the final decade of analysis (e.g., where 2100 is calculated as 2091-2100) in each climate scenario.

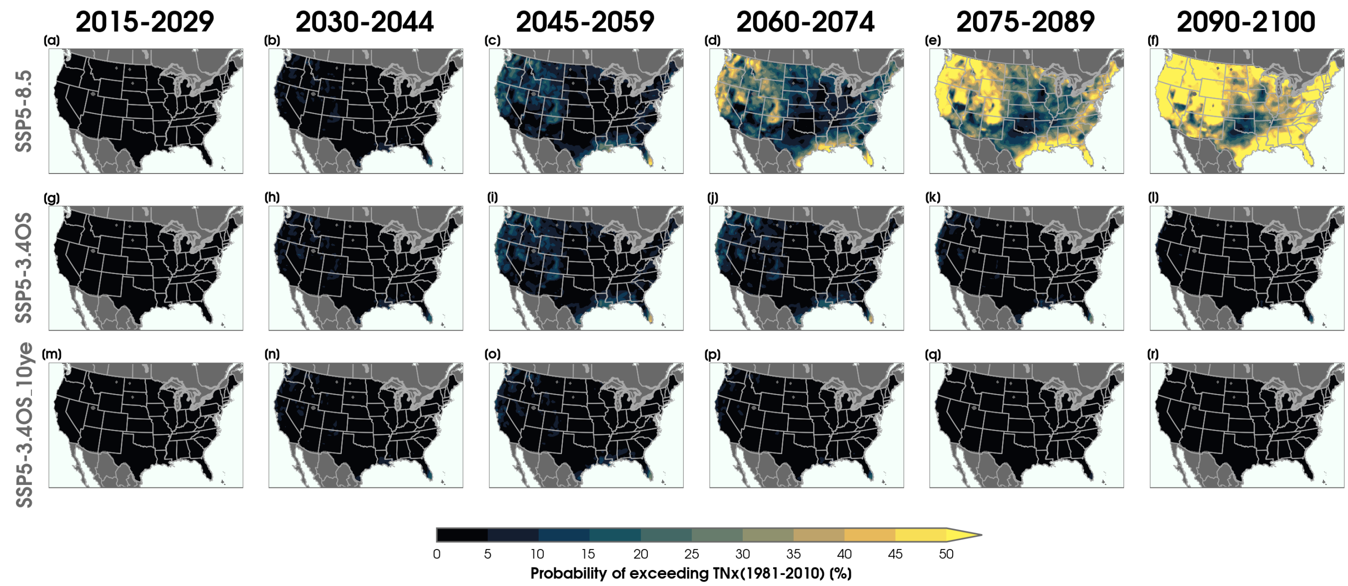


**Figure S6.** (a) Probability of a month having at least one day that exceeds the JJA highest nighttime minimum temperature (TNx) for SSP5-8.5 in 2015 to 2029, (b) 2030 to 2044, (c) 2045 to 2059, (d) 2060 to 2074, (e) 2075 to 2089, and (f) 2090 to 2100. (g-l) Same as (a-f), but for SSP5-3.4OS. (m-r) Same as (a-f), but for SSP5-3.4OS_10ye. Note that the data for the years from 2015 to 2030 are taken from SSP5-3.4OS in this row. The TNx threshold is calculated separately at each grid point over the 1981 to 2010 reference period by considering all ensembles in the historical scenario and across all days in the months of JJA. The probabilities are calculated by considering all ensemble members and months per each epoch for the respective climate scenarios.

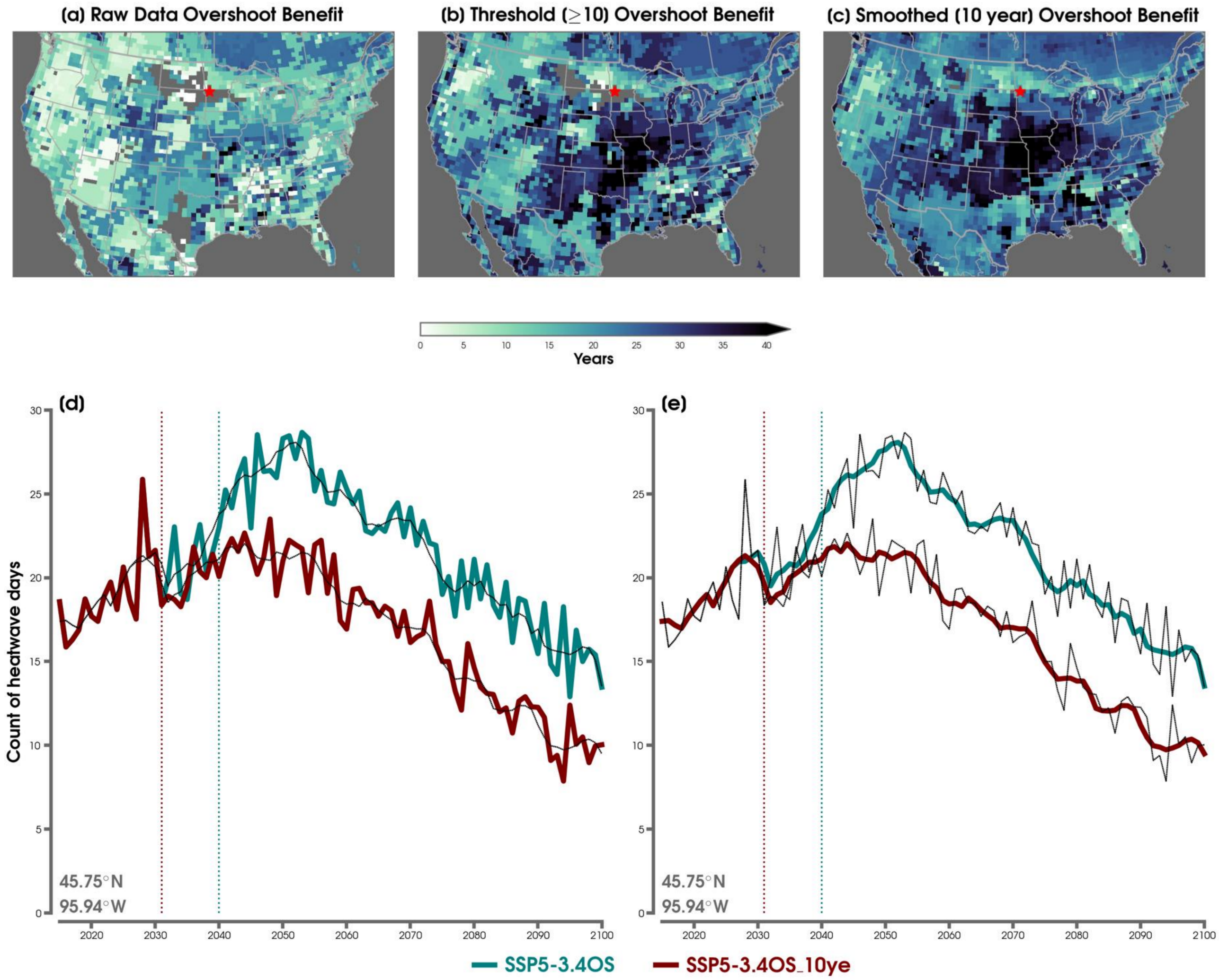


**Figure S7.** (a) Map of the raw differences in years between when the maximum number of Tx90 summer days is reached for the ensemble mean of SSP5-3.4OS_10ye compared to the year that the ensemble mean of SSP5-3.4OS first falls below this maximum after its peak in $CO_2$ concentrations. This is calculated at each grid point. Locations with no positive difference in years according to this definition are masked out in gray. A blue star highlights the location of the example in (d-e). (b) Same as (a), but for the first year in SSP5-3.4OS when at least the next 10 years remain consistently below this maximum number of Tx90 days in SSP5-3.4OS_10ye. (c) Same as (a), but after applying a Savitzky-Golay filter (Savitzky and Golay, 1964) with a 10-year smoothing window (3rd order polynomial) to the ensemble mean count of Tx90 at each grid point and for each respective climate scenario. (d) An example of this methodology for a location in western Minnesota (approximately 45.75°N and 95.94°W) showing the time series of the count of Tx90 summer days in SSP5-3.4OS_10ye (dark red line) and SSP5-3.4OS (dark green line) from 2015 to 2100. The thin dashed black line shows the time series after applying the Savitzky-Golay smoothing filter. Dashed vertical lines are shown for the start of climate mitigation in SSP5-3.4OS_10ye (dark red; 2031) and SSP5-3.4OS (dark green; 2040). (e) Same as (d), but after applying the Savitzky-Golay filter to the time series of SSP5-3.4OS_10ye (dark red line) and SSP5-3.4OS_10ye (dark green line). The raw data for each climate scenario from panel (d) is also shown with a thin dashed black line.

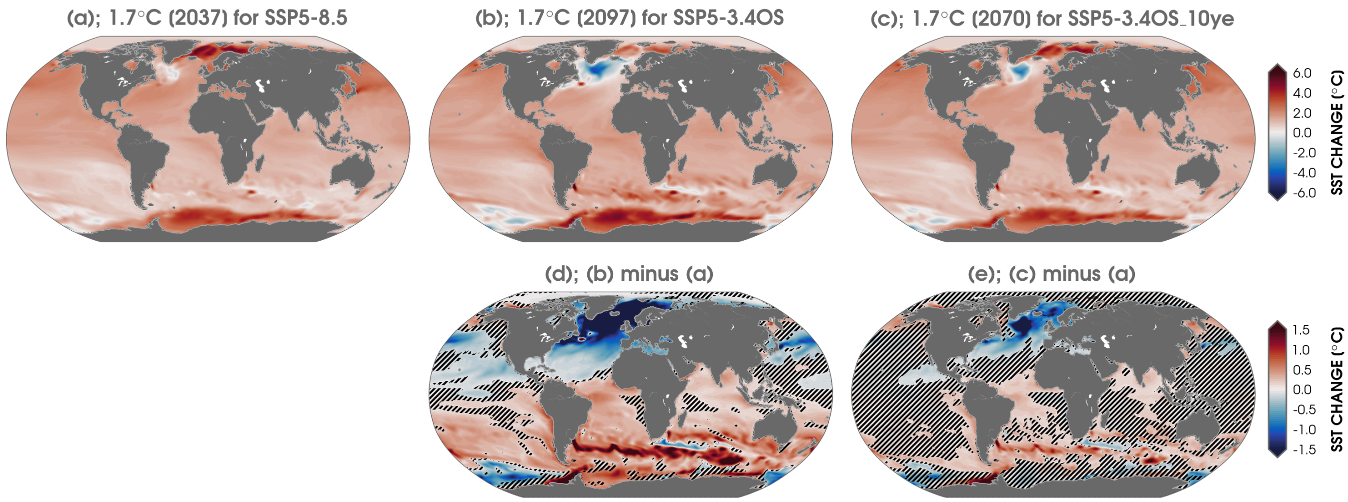


**Figure S8.** Same as Figure S4, but for global composites of sea surface temperature (SST) change.

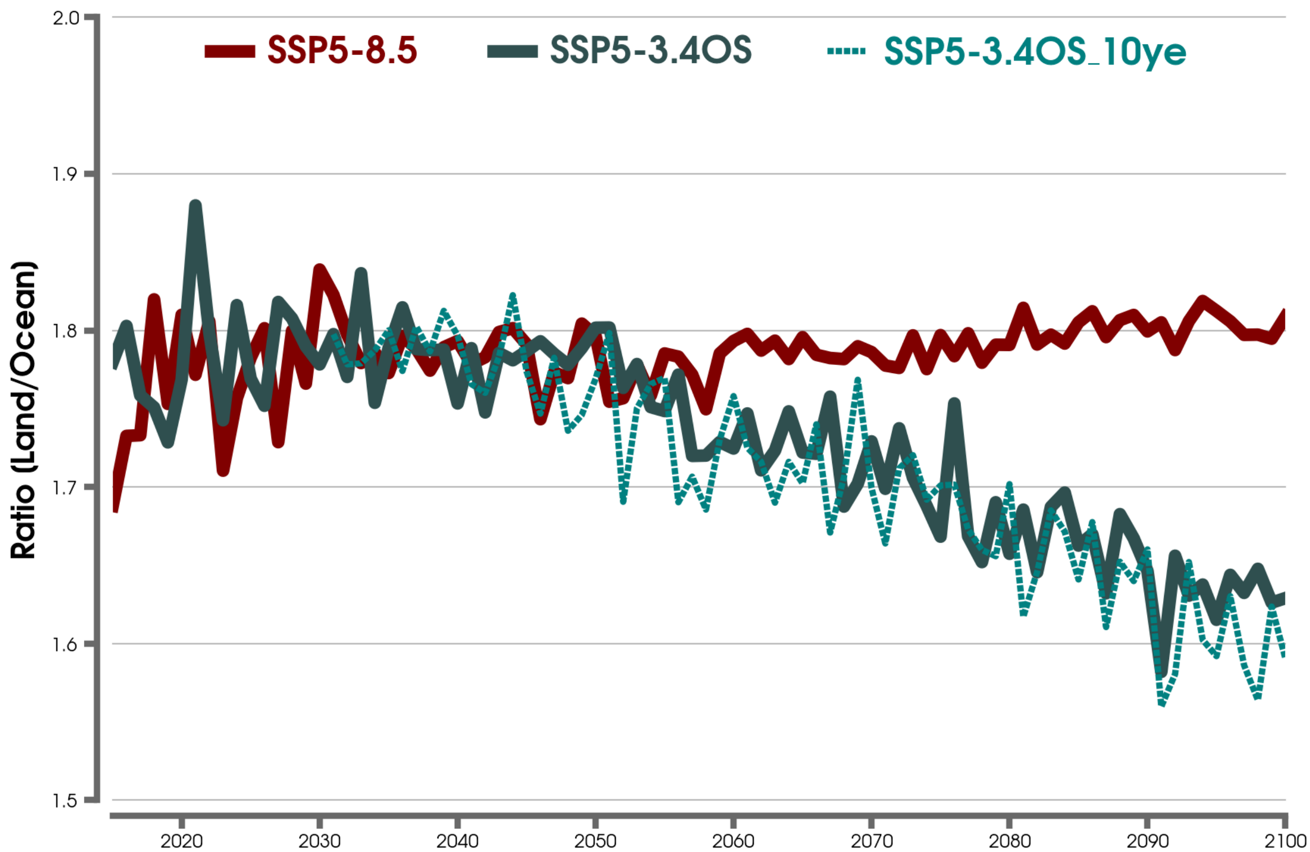


**Figure S9.** (a) Time series of the mean global land-sea temperature ratio over the months of JJA from 2015 to 2100 for the ensemble mean of SPEAR following the SSP5-8.5 future climate scenario from 2015 to 2100 (solid dark red line), the SSP5-3.4OS future climate scenario from 2015 to 2100 (solid dark green line), and from 2031 to 2100 for the SSP5-3.4OS_10ye climate scenario (thin dashed light green line). Anomalies are first computed with respect to their 1921-1950 climatological time means using the SPEAR historical scenario. Near-surface air temperatures (2 m height) are used for over land areas, and sea surface temperatures are used for over ocean areas.

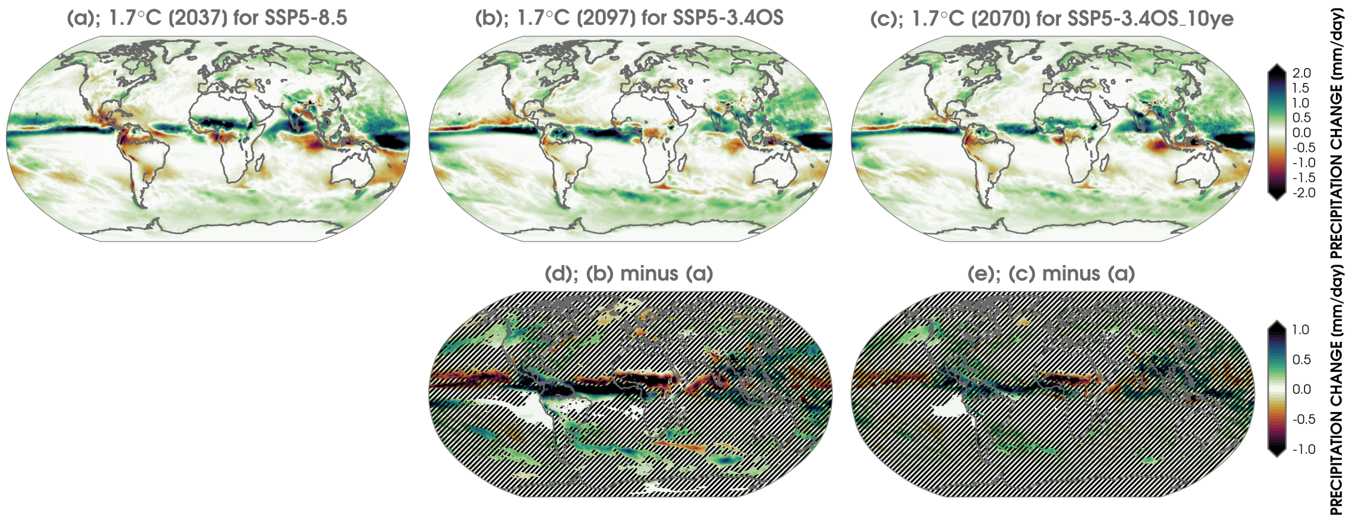


**Figure S10.** Same as Figure S8, but for composites of precipitation change.

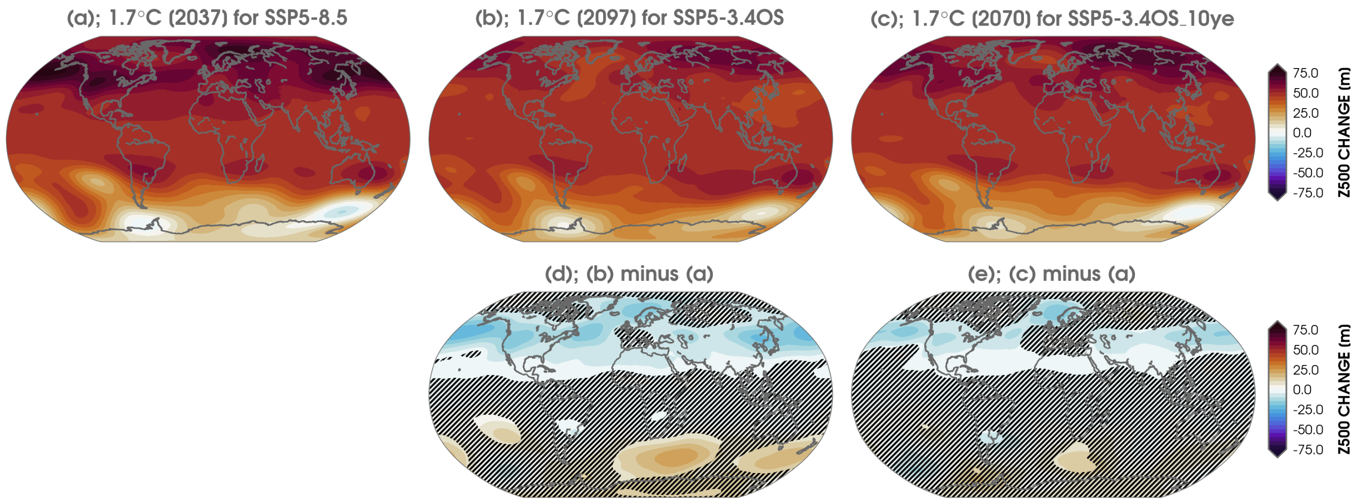


**Figure S11.** Same as Figure S8, but for composites of geopotential height at 500 hPa (Z500) change.

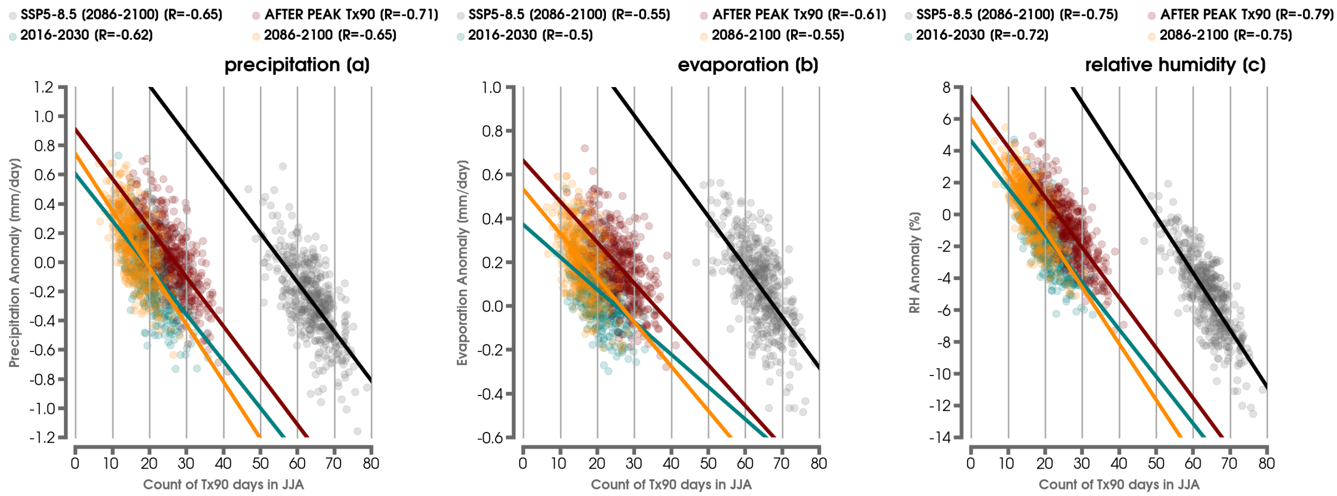


**Figure S12.** (a) The relationship of changes in mean precipitation relative to the number of Tx90 days in JJA averaged across CONUS for the SSP5-8.5 climate scenario in 2086 to 2100 (gray dots). This relationship is also shown for the SSP5-3.4OS_10ye climate scenario in years 2025 to 2039 (blue dots), the 15 years after the ensemble mean's highest count of Tx90 days in SSP5-3.4OS_10y (orange dots), and for the 2086 to 2100 period in SSP5-3.4OS (dark red dots). Anomalies are computed with respect to their 1921 to 1950 climatological mean. The scatter points consider all years and ensemble members for each epoch period. A solid line is displayed for the linear least squares fit along with its corresponding Pearson correlation coefficient (R) listed in the legend. (b) Same as (a), but for Tx days related to changes in mean evaporation, (c) Same as (a), but for Tx days related to changes in mean relative humidity. All correlations are statistically significant at $p < 0.01$.

## Section S3. References:

Benjamini, Y. and Hochberg, Y. (1995). Controlling the false discovery rate: A practical and powerful approach to multiple testing, *Journal of the Royal Statistical Society: Series B (Methodological)* **57**.

Delworth, T. L., Cooke, W. F., Adcroft, A., Bushuk, M., Chen, J.-H., Dunne, K. A., Ginoux, P., Gudgel, R., Hallberg, R. W., Harris, L., Harrison, M. J., Johnson, N., Kapnick, S. B., Lin, S.-J., Lu, F., Malyshev, S., Milly, P. C., Murakami, H., Naik, V., Pascale, S., Paynter, D., Rosati, A., Schwarzkopf, M., Shevliakova, E., Underwood, S., Wittenberg, A. T., Xiang, B., Yang, X., Zeng, F., Zhang, H., Zhang, L. and Zhao, M. (2020). Spear: The next generation gfdl modeling system for seasonal to multidecadal prediction and projection, *Journal of Advances in Modeling Earth Systems* **12**: e2019MS001895.
**URL:** *https://agupubs.onlinelibrary.wiley.com/doi/10.1029/2019MS001895*

Labe, Z. M., Delworth, T. L., Johnson, N. and Cooke, W. F. (2024). Exploring a data-driven approach to identify regions of change associated with future climate scenarios, *ESS Open Archive* pp. 1–61.
**URL:** *https://doi.org/10.22541/essoar.171288901.17027965/v1*

Savitzky, A. and Golay, M. J. (1964). Smoothing and differentiation of data by simplified least squares procedures, *Analytical Chemistry* **36**.

Wilks, D. S. (2006). On “field significance” and the false discovery rate, *Journal of Applied Meteorology and Climatology* **45**: 1181–1189.
**URL:** *http://journals.ametsoc.org/doi/abs/10.1175/JAM2404.1*

Wilks, D. S. (2016). “the stippling shows statistically significant grid points”: How research results are routinely overstated and overinterpreted, and what to do about it, *Bulletin of the American Meteorological Society* **97**: 2263–2273.
**URL:** *http://journals.ametsoc.org/doi/10.1175/BAMS-D-15-00267.1*